Fate conversion mediates restoration of mature GABAergic neuronal identity in Huntington's disease

Lee, Siwoo

Department of Biomedical Engineering

Graduate School

Yonsei University

Fate conversion mediates restoration of mature GABAergic neuronal identity in Huntington's disease

Advisor Cho, Sung-Rae

A Master's Thesis Submitted
to the Department of Biomedical Engineering
and the Committee on Graduate School
of Yonsei University in Partial Fulfillment of the
Requirements for the Degree of
Master of Biomedical Engineering

Lee, Siwoo

June 2025

Fate conversion mediates restoration of mature GABAergic neuronal identity in Huntington's disease

This Certifies that the Master's Thesis of Lee, Siwoo is Approved

Committee Chair _____

Cho, Sung-Rae

Committee Member _____

Kim, Hyongbum

Committee Member _____

Kim, Daesik

Department of Biomedical Engineering
Graduate School
Yonsei University
June 2025

ACKNOWLEDGEMENTS

As I bring this research journey to a close, I would like to take this opportunity to express my sincere gratitude to everyone who has accompanied me along the way. This experience has reminded me once again that academic pursuits are never achieved through individual effort alone.

I am deeply grateful to my advisor, Professor Sung-Rae Cho, who helped me regain my direction whenever I felt lost amidst the cycle of reasoning and experimentation. His trust and measured guidance have not only shaped my academic attitude but also taught me how to view the world through the eyes of a researcher.

I would also like to thank my lab colleagues with whom I spent countless hours conducting experiments and engaging in discussions. The moments we shared while navigating complex problems and exchanging perspectives have been invaluable. These experiences have taught me the importance of solidarity and balance within a research community, and they will continue to serve as a foundation for both my academic and personal growth.

Above all, I extend my heartfelt thanks to Dr. Seongmoon Jo, Dr. Dong Joo Yang and Dr. Khanh V Doan, who patiently and tirelessly taught me from the very beginning when I knew nothing. Despite my repeated questions, they always responded with sincerity and never hesitated to help me with even the smallest of difficulties. I will never forget their generosity.

I am also deeply grateful to my family and friends who silently supported me throughout this process, and especially to Dr. Junwon Park, who was always there for me with quiet encouragement. The support I received from those who understand how many small decisions and sacrifices are required to complete something meaningful will remain in my memory far longer than the outcome itself.

This research has meant more to me than a mere academic result. In following a single question to the very end, I have relearned how to ask the right questions and have gained the ability to discern when to pause and when to persevere. This experience will remain as clear evidence of my growth, far beyond the conferral of a degree.

Though these words may not fully capture the depth of my gratitude and respect, I hope the sincerity behind them will be remembered for a long time.

ACKNOWLEDGEMENTS

하나의 연구 여정을 마무리하며, 이 자리를 빌려 그 과정에 함께해 주신 모든 분들께 진심으로 감사의 마음을 전합니다.

학문은 언제나 개인의 힘만으로 이루어지지 않는다는 사실을 다시금 실감한 시간이었습니다. 다양한 사유와 실험의 반복 속에서 방향을 잃을 때마다, 제게 중심을 잡아주신 지도교수님 조성래 교수님께 깊이 감사드립니다. 교수님께서 보여주신 신뢰와 절제된 지도는 제게 학문에 대한 태도뿐 아니라 연구자로서 지녀야 할 시선을 가르쳐 주셨습니다.

또한, 연구실 동료들과 함께 실험하고 토론하며 보낸 시간은 저에게 큰 자산이 되었습니다. 복잡한 문제 앞에서 서로의 관점을 나누고 협력했던 경험은 공동체 속에서 배우는 연대감과 균형의 가치를 일깨워 주었고, 이는 앞으로도 제 학문적 · 인격적 성장에 중요한 밑거름이 될 것입니다.

무엇보다도 아무것도 몰랐던 시절부터 인내심을 갖고 끊임없이 가르쳐 주신 재활의학과 조성문 선생님, 구강생물학교실 양동주 박사님, 그리고 Khanh 박사님께 깊은 감사의 인사를 전합니다. 같은 질문을 수없이 반복했음에도 늘 진심 어린 답을 주시고, 사소한 어려움에도 아낌없는 도움을 주신 은혜를 잊지 않겠습니다.

아울러, 이 과정을 묵묵히 지켜봐 주며 응원해 준 가족과 친구들, 그리고 누구보다 가까운 자리에서 조용히 응원해 주신 신경외과 박준원 선생님께도 깊이 감사드립니다. 무언가를 완성해 나간다는 것이 얼마나 많고 작은 선택과 단념 위에 세워지는지를 아는 이들로부터 받은 응원은, 결과보다 더 오래 기억에 남을 것 같습니다.

이번 연구는 제게 단순한 결과물 이상의 의미였습니다. 하나의 의문을 끝까지 밀고 나가는 과정에서 질문하는 법을 다시 배우고, 멈춰야 할 순간과 끝까지 가야 할 지점을 스스로 구분할 수 있게 되었습니다. 이러한 경험은 학위 취득을 넘어, 제 성장의 확실한 증거로 남을 것입니다.

비록 이 글이 모든 고마움과 존경을 온전히 담아내지는 못하겠지만, 그 마음만큼은 오래도록 기억되기를 바랍니다. 감사합니다.

TABLE OF CONTENTS

LIST OF FIGURES

LIST OF TABLES

ABSTRACT

Fate conversion mediates restoration of mature GABAergic neuronal identity in Huntington's disease

The striatum comprises two transcriptionally and functionally distinct compartments—striosomes and matrix— each playing unique roles in cortical input processing, dopamine receptor signaling, and motor/emotional regulation. Among these, D2 receptor-expressing striosomal medium spiny neurons (MSNs) are central components of the indirect pathway and are selectively and early degenerated in Huntington's disease (HD), contributing to mood and behavioral impairments. In this study, we evaluated the potential of astrocyte-to-neuron reprogramming to restore striatal GABAergic MSNs in the R6/2 HD mouse model was assessed, comparing both Ascl1 and NeuroD1 transcription factors in terms of reprogramming mechanism and subtype specificity. This work is organized into three parts:

Part 1 demonstrates that Ascl1 suppressed reactive astrocyte markers (GFAP and C3) and promoted the expression of GABA and DARPP-32, thereby facilitating a GABAergic neuronal fate. Single-nucleus RNA sequencing (snRNA-seq) revealed the emergence of immature D2 striosomal progenitor clusters the express Meis2, Epha5, and Dlx1. BrdU-based lineage tracing confirmed that these neurons originated from dividing astroglial precursors, indicating that Ascl1 acts via an indirect, progenitor-like reprogramming route.

Part 2 exhibits that NeuroD1 enabled rapid and direct astrocyte conversion into mature GABAergic MSNs, spanning both striosomal and matrix identities. Behavioral analyses (rotarod, grip strength, and clasping) revealed significant functional recovery in NeuroD1-treated mice. Increased KCC2 expression supported the restoration of chloride homeostasis and potential circuit integration.

Taken together, these results revealed that Ascl1 selectively restores D2 striosomal MSNs, which are crucial for the indirect pathway, whereas NeuroD1 promotes a broader recovery of MSN subtypes, accompanied by significant improvements in motor function. Comparative analyses in Part 3 revealed that these two transcription factors act via distinct yet complementary mechanisms, wherein Ascl1 primarily re-establishes compartmental identity and NeuroD1 facilitates earlier

circuit-level recovery, thereby highlighting the therapeutic potential of tailored astrocyte-to-neuron reprogramming strategies for striatal circuit repair in HD.

Collectively, this study demonstrated that astrocyte-to-neuron reprogramming offers a viable approach for restoring striatal circuitry in HD and provides a conceptual basis for developing subtype-specific and disease-stage-tailored regenerative therapies.

Key words : Huntington’s disease, astrocyte-to-neuron conversion, striosome, matrix, indirect pathway

1. INTRODUCTION

The striatum, the primary input nucleus of the basal ganglia, plays a crucial role not only in motor control but also in emotion, motivation, and decision-making. Its principal neuronal subtype, the medium spiny neuron (MSN), can be categorized into two major classes based on dopamine receptor expression: D1- and D2-type MSNs. D1-type MSNs, which form the direct pathway and promote movement initiation through projections to the internal globus pallidus and substantia nigra pars reticulata, whereas D2-type MSNs form the indirect pathway via the external globus pallidus to suppress competing or inappropriate motor programs[11, 12, 13].

MSNs are not uniformly distributed throughout the striatum but instead segregate into two anatomically and molecularly distinct compartments: striosomes and matrix[5]. These compartments differ in terms of their developmental origin, gene expression profiles, connectivity, and functional roles[4, 7, 8]. The matrix compartment comprises the majority of the striatal volume and is primarily associated with sensorimotor processing and execution of learned behaviors via the classical cortico–basal ganglia–thalamo–cortical loop[8, 9]. In contrast, striosomes are smaller, patch-like domains enriched in neurons that receive inputs from limbic and prefrontal areas and directly project to dopaminergic neurons in the substantia nigra pars compacta (SNc)[2, 3]. Through this connection, striosomal neurons exert top-down modulation over dopamine release, thereby indirectly regulating the activity of the surrounding matrix circuitry[2, 4].

Functionally, striosomes may act as hierarchical controllers that assign emotional or motivational value to actions, which identify “what to do,” whereas the matrix implements “how to do it”[3, 4]. Both D1- and D2-type MSNs exist in both compartments. However, striosomal neurons exhibit distinct transcriptional signatures and display circuit integration patterns that significantly differ from those of their matrix counterparts[1, 6, 8]. These are immature striosome markers for the mature striosome compartment, such as MOR/Oprm1, Pbx3, Tshz1, and Kcnip1, which do not differentiate the striosome compartment alone.

These characteristics indicate that striosomes are not just anatomical curiosities but functional subunits that are crucial for behavior selection and adaptive learning[3, 4].

Selective vulnerability of MSNs causes profound disruptions to basal ganglia circuitry in Huntington's disease (HD), a progressive neurodegenerative disorder caused by an expanded CAG repeat in the *HTT* gene[1, 17]. D2-type MSNs are known to deteriorate earlier than D1-type MSNs; however, recent evidence indicates that D2-expressing striosomal neurons are among the earliest affected cell types[1, 3, 16]. This early loss disrupts inhibitory control over SNc dopaminergic neurons, resulting in aberrant dopamine release and subsequent dysregulation of matrix activity[2, 3, 14]. D1 striosomal neurons, followed by D2 and D1 matrix neurons, are also lost as the disease progresses. This cascade of degeneration follows a specific sequence: D2 striosome → D1 striosome → D2 matrix → D1 matrix[1, 13].

This temporally and spatially ordered degeneration aligns with the clinical progression of HD, where cognitive and psychiatric symptoms, such as impulsivity, affective dysregulation, and impaired decision-making, often precede overt motor impairments. Despite their functional significance, D2 striosomal neurons remain poorly understood in terms of molecular identity, developmental trajectory, and susceptibility to degeneration. More importantly, effective strategies for selectively replacing or repairing these neurons are currently unavailable[1, 17, 18].

Recent advances in direct neuronal reprogramming have provided novel opportunities for circuit repair[18–22]. In some cases, transcription factors, such as Ascl1 and NeuroD1, have been shown to convert astrocytes into neurons both *in vitro* and *in vivo*, bypassing intermediate progenitor states[19, 20, 22]. However, whether such reprogramming can be directed toward specific neuronal subtypes, such as D2 striosomal MSNs, remains unclear.

This study investigates whether forced expression of Ascl1 or NeuroD1 in striatal astrocytes can induce transcriptional reprogramming toward a D2 striosomal fate. Further, it examines whether the reprogrammed neurons functionally integrate into striosome-associated circuits and contribute to the restoration of striatal function in an HD mouse model.

This study introduces a novel therapeutic strategy that targets the earliest dysfunctional nodes in the striatal network—specifically, the loss of D2 striosomal neurons—and ultimately promotes meaningful recovery in HD by focusing on subtype-specific reprogramming and circuit-level restoration[1, 17, 31].

2. MATERIALS AND METHODS

2.1. Primary Cell Isolation

Neonatal mice (3-5 days old) were euthanized and both cortices were aseptically dissected and placed in Hank's Balanced Salt Solution. The cortical tissue was then dissociated into a single-cell suspension by repeated pipetting in Dulbecco' modified Eagle's medium (DMEM)/Ham's F-12 medium supplemented with 10% fetal bovine serum (FBS), 1% penicillin/streptomycin, 1× MEM Non-Essential Amino Acids solution, sodium pyruvate, and 1× 200 mM L-glutamine. The suspension was homogenized, strained, and rinsed with Dulbecco's PBS before being seeded in a T-75 flask and incubated at 37°C with medium changes every 3-4 days. After 7 days, the culture was shaken for at least 6 h, and the supernatant was removed. The cells were then treated with 0.25% Trypsin-EDTA for 10 min at 37°C to detach them. The cells were used for subsequent experiments.

2.2. Primary Astrocyte Transfection

Adherent cells in T-75 flasks were grown sufficiently, washed with PBS, treatmed with 0.05% trypsin at 37°C for 5 min to detach the cells. The detached cells were collected in the growth medium, with the suspension adjusted to 1x105 cells/mL. Aliquots of 1ml of aliquots was dispensed in each well of a 4-well plate (30104; SPL Life Sciences, Seoul, Korea) and incubated at 37°C in an atmosphere of 5% CO2 for 24 h. For transfection, 200 μL of Opti-MEM™ was prepared and left static at room temperature for 5 min prior to the addition of AAV4 (multiplicity of infection = 1), 7 μL Lipofectamine® 2000 reagent, and F-12 FBS-containing medium. The preparation was incubated at room temperature for 20 min then added dropwise to the cells in a 6-well plate, with gentle rocking to ensure uniform distribution. After 24 h, the culture medium was replaced with fresh medium, and the cells were incubated for an additional 24 h.

2.3. Experimental timeline of study

Mice were randomly assigned to one of four groups: Control (N = 8), AAV9-Null (N = 7), AAV9-Ascl1 (N = 7), or AAV9-NeuroD1 (N = 11).

At postnatal week 3, baseline behavioral assessments—including the rotarod, clasping, and grip strength tests—were conducted.

In week 4, viral vectors were delivered into the striatum via stereotaxic injection. Following the injection, the mice were monitored for a total of 8 weeks. During this period, rotarod and clasping tests were performed weekly to track motor function, while grip strength and open field tests were administered as final evaluations in week 12.

At the end of the 12-week period, the animals were euthanized, and brain tissues collected at both 8 and 12 weeks post-injection were subjected to molecular and histological analyses.

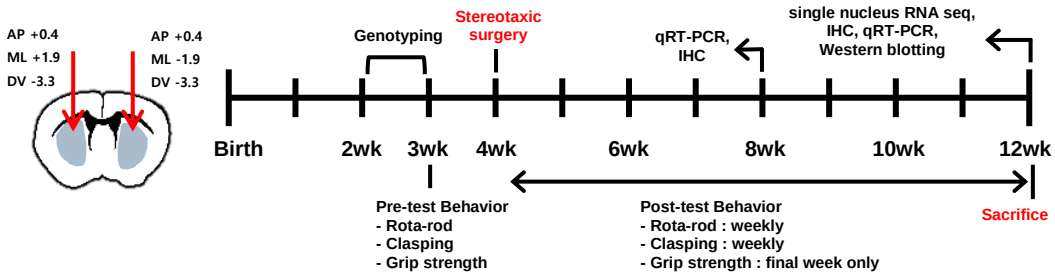

Figure 1. Timeline of in vivo experimental procedures

AAV9 vectors were stereotactically injected at 4 weeks of age (Week 0). Behavioral assessments were performed before injection (Week –1) and weekly thereafter. The rotarod and clasping tests were conducted every week, while the grip strength test was performed only in the final week (Week 8 or Week 12). Brain tissues were collected at Weeks 8 and 12 for molecular and histological analyses.

2.4. Stereotaxic Injection

At postnatal week 4, mice were anesthetized via intraperitoneal (IP) injection of ketamine (100 mg/kg; Huons, Gyeonggi-do, Korea) and xylazine (10 mg/kg; Bayer Korea, Seoul, Korea).

After securing the mice in a stereotaxic apparatus, 1 μL of AAV9 viral vector was injected into each hemisphere of the striatum (total of 2 μL per mouse). The stereotaxic coordinates used for the injection were 0.4 mm anterior (AP), ±1.9 mm lateral (ML), and 3.3 mm ventral (DV) from the dura, relative to the bregma.

All injections were performed using a 10 μL Hamilton syringe with a glass micropipette tip, and the injection rate was controlled at 0.2 μL/min. The needle was left in place for 5 minutes after injection to minimize backflow before being slowly withdrawn.

2.5. AAV9 Viral Vector

In this study, recombinant AAV9 viral vectors were employed to drive astrocyte-specific gene expression under the control of the GFAP promoter. Each construct included a WPRE (woodchuck hepatitis virus post-transcriptional regulatory element) and BGH polyA sequence to enhance transgene expression and stability.

- The control vector (VB211011-1357txv) expresses EGFP.
- The Ascl1 vector (VB211011-1354sju) expresses mouse Ascl1 (NM_008553.5) with an HA tag.
- The NeuroD1 vector (VB211011-1356swm) expresses mouse NeuroD1 (NM_010894.3) with a 3×FLAG tag.

All vectors were produced by VectorBuilder (Chicago, IL, USA) and purified using the iodixanol gradient method. The vectors were packaged into AAV9 capsids with a final titer of 1×10^9 vg/μL.

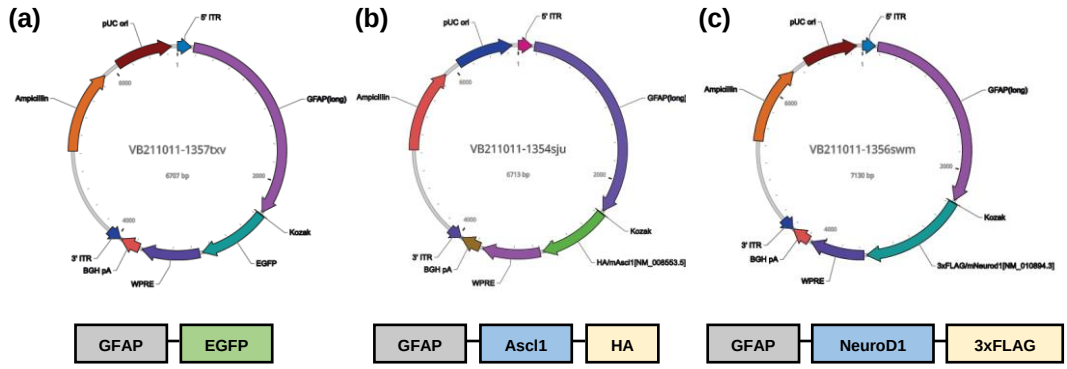

Figure 2. Schematic diagrams of AAV9 viral vector constructs

(A) Control vector expressing EGFP under the GFAP promoter. (B) Ascl1 vector expressing HA-tagged mouse Ascl1. (C) NeuroD1 vector expressing 3×FLAG-tagged mouse NeuroD1. All vectors include WPRE and BGH polyA sequences to enhance transgene expression and stability.

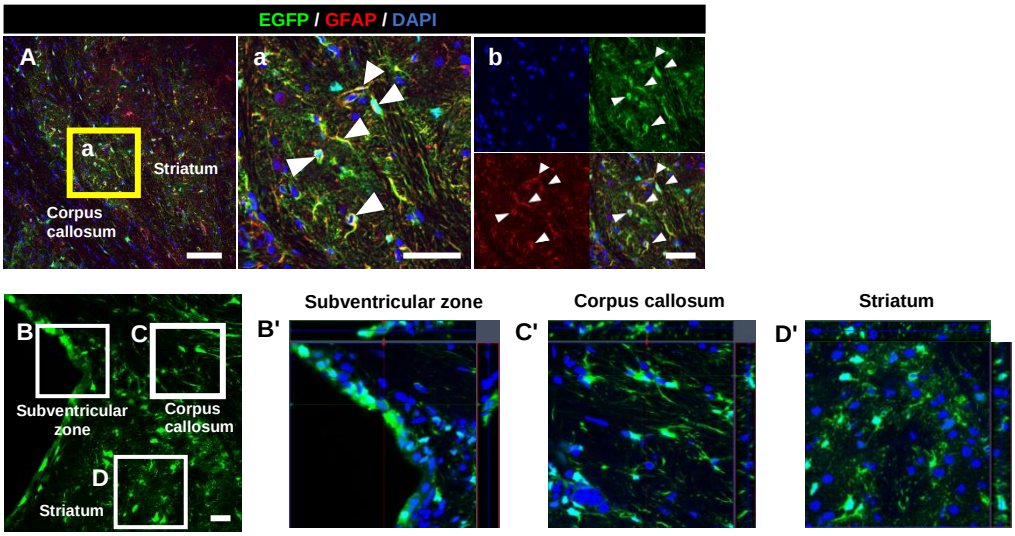

Figure 3. Regional expression pattern of EGFP under the GFAP promoter across brain regions following AAV delivery

(A) Representative low-magnification image showing EGFP (green), GFAP (red), and DAPI (blue) expression in the striatum and corpus callosum. (a) Enlarged image of the boxed area in (A), showing GFAP+ astrocytes co-expressing EGFP (arrowheads), indicating astrocyte-specific targeting. (b) Separate and merged channels of the boxed region showing colocalization of EGFP and GFAP signals. (B–D) Low-magnification images showing EGFP expression across different brain regions: subventricular zone (B), corpus callosum (C), and striatum (D). (B'–D') Higher magnification of the corresponding regions in (B–D) showing EGFP expression in GFAP+ cells in each area. Colocalization indicates astrocyte-specific expression of the virus in all examined regions. Scale bars: A = 100 μm; a, b = 50 μm; B–D = 20 μm.

2.6. Animal model

In this study, we utilized the R6/2 transgenic mouse model of Huntington's disease (HD), which expresses exon 1 of the human HTT gene containing approximately 160 ± 5 CAG repeats. These mice were obtained from the Jackson Laboratory (Bar Harbor, ME, USA; B6CBA-Tg(HDexon1)62Gpb/1J, Stock No: 002810). The R6/2 line exhibits a broad range of neurological abnormalities that recapitulate symptoms seen in human HD, including choreiform movements, involuntary stereotypies, tremors, seizures, and abnormal vocalizations. Symptoms typically begin to appear between 6 and 8 weeks of age, and the mice have an average lifespan of around 12 weeks. To alleviate potential dehydration and malnutrition during the late stages of disease progression, we provided water-soaked food pellets daily.

All animals were housed in an AAALAC-accredited facility, and all procedures were conducted in accordance with protocols approved by the Institutional Animal Care and Use Committee (IACUC 2022-0205, 2024-0061). Mice were maintained under a 12-hour light/dark cycle in a temperature-controlled environment with free access to food and water. To assess the effects of AAV-mediated gene expression on HD pathology, animals were assigned to the following groups: Control (untreated), viral control expressing EGFP, and experimental groups expressing either Ascl1 or NeuroD1. This study also included an analysis of therapeutic effects at various time points, including the 8-week time point, to evaluate the temporal dynamics of intervention outcomes.

2.7. Immunocytochemistry

Immunocytochemistry was carried out based on previously described methods with minor modifications. Briefly, cultured cells were fixed in 4% paraformaldehyde for 10 minutes and permeabilized with 0.1% Triton X-100 in PBS for 15 minutes at room temperature. After blocking with 5% bovine serum albumin for 1 hour, the cells were incubated overnight at 4°C with the following primary antibodies (1:400 dilution): GFAP (RA-22101; Neuronomics), GABA (A2052; Sigma-Aldrich), DARPP-32 (sc-271111;

Santa Cruz Biotechnology), and NeuN (MAB377; Millipore). After three PBS washes, cells were incubated with Alexa Fluor 488- or 594-conjugated secondary antibodies (Thermo Fisher Scientific) for 1 hour at room temperature. Nuclei were counterstained with Hoechst 33342 (10 μg/mL in PBS; Thermo Fisher Scientific), and fluorescence images were obtained using a confocal laser scanning microscope (LSM700; Carl Zeiss).

2.8. Immunohistochemistry

Following stereotaxic injection, mice received daily intraperitoneal injections of BrdU (50 mg/kg; Sigma-Aldrich, St. Louis, MO, USA) for 12 consecutive days. At 12 weeks of age, R6/2 mice were euthanized and perfused transcardially with cold 1× PBS, followed by 4% paraformaldehyde. Brains were harvested, embedded in sectioning compound (Leica, Wetzlar, Germany), rapidly frozen in isopentane, and cryosectioned at 16 μm thickness using a Cryostat Leica 1860 cryomicrotome (Leica Biosystems Italia, Buccinasco MI, Italy). Four representative sections per brain, spanning over 128 μm, were selected for immunohistochemistry.

Tissue sections were stained with the following primary antibodies: BrdU (ab6326, 1:200; Abcam) and Ki67 (ab16667, 1:400; Abcam) for proliferating cells; NeuN (MAB377, 1:400; Millipore), DARPP-32 (sc-271111; Santa Cruz Biotechnology), and GABA (A2052, 1:400; Sigma-Aldrich) for neuronal markers; GFAP (RA-22101, 1:400; Neuronomics) for astrocytes; and PBX3 (12571-1-AP, 1:200; Proteintech) and EPHA4 (21845-1-AP, 1:400; Proteintech) for developmental and axonal guidance markers.

2.9. RNA Preparation

Total RNA was extracted from in vitro and in vivo samples using TRIzol reagent (Thermo Fisher Scientific, Waltham, MA, USA) in accordance with the manufacturer's protocol. The concentration and purity of the isolated RNA were assessed using a NanoDrop spectrophotometer (Thermo Fisher Scientific).

2.10. Quantitative Real-Time Reverse Transcription-Polymerase Chain Reaction

Quantitative real-time PCR (RT-qPCR) was conducted to validate the transcriptomic data. Complementary DNA (cDNA) was synthesized from total RNA using the ReverTra Ace® qPCR RT Master Mix with gDNA Remover (Toyobo, Osaka, Japan), following the manufacturer's protocol. RT-qPCR was performed with qPCRBIO SyGreen Mix Hi-ROX (PCR BIOSYSTEMS, London, UK) on a StepOnePlus Real-Time PCR System (Applied Biosystems, Foster City, CA, USA) to quantify the mRNA expression levels of target genes. Relative gene expression was calculated using the $2^{-\Delta\Delta C_T}$ method. Primer sequences used for the assays are listed in Table S1.

2.11. Western blot

Total protein was extracted from cultured cells and mouse tibia using RIPA buffer (Thermo Fisher Scientific, Waltham, MA, USA) according to the manufacturer's instructions. Equal amounts of protein (30 μg per sample) were separated by electrophoresis on a 10% SDS–polyacrylamide gel (Bio-Rad Laboratories, Richmond, CA, USA) and transferred to 0.45 μm PVDF membranes (Amersham Pharmacia Biotech, Little Chalfont, UK). Membranes were blocked with 5% BSA and then incubated overnight at 4 °C with primary antibodies against KCC2 (1:1000; Cell Signaling Technology, 94705S) and NKCC1 (1:1000; Santa Cruz Biotechnology, sc-514774). After washing, membranes were incubated for 1 hour with horseradish peroxidase-conjugated secondary antibodies (1:3000; Santa Cruz Biotechnology). Protein bands were visualized using the Amersham ImageQuant 800 imaging system (Cytiva, Marlborough, MA, USA).

2.12. Single Nucleus RNA sequencing (snRNA-seq)

Striatal tissues were collected 8 weeks after AAV9-GFAP vector injection in R6/2 Huntington's disease model mice. Nuclei were isolated using Nuclei EZ Lysis buffer (Sigma), and viable nuclei were selected via DAPI staining followed by FACS. Library

preparation and sequencing were outsourced to Macrogen (Seoul, Korea), using the Chromium GEM-X Single Cell 3′ RNA Library Kit v4 (10x Genomics). Sequencing was performed on the Illumina NovaSeq 6000 platform with paired-end reads.

2.13. Bioinformatics Analysis

Raw FASTQ files were processed using Cell Ranger (v8.0.1, 10x Genomics) and aligned to the mm10 (GRCm39) reference genome. Downstream analysis was performed in R (v4.4.3) using the Seurat package (v5.0.0). Cells were filtered using the following criteria: percent.mt < 5, nFeature_RNA > 200, and nCount_RNA < 8000. The data was normalized using the NormalizeData() function, followed by dimensionality reduction via principal component analysis (PCA). Clustering was performed using FindNeighbors(dims = 1:15), FindClusters(resolution = 0.5), and RunUMAP(dims = 1:15).

Cell type annotation was conducted using scType (Ianevski et al., 2022). Mature GABAergic neurons were selected based on scType annotation and used for downstream analysis in Parts 1 and 2. For broader comparative analysis, clusters annotated as GABAergic neurons, glutamatergic neurons, immature neurons, neuronal progenitors, oligodendrocyte progenitors, and mature neurons were selected. These clusters were reclustered using the same parameters as above. GABAergic clusters were manually validated by coexpression of canonical GABAergic markers (Slc6a1, Gabbr1, Gabbr2, Gad1, Gad2, Slc32a1) and exclusion of canonical markers of other cell types (e.g., Slc17a7 for glutamatergic neurons). GABAergic MSNs were further subclassified based on the expression of MSN identity markers (Bcl11b, Foxp2, Foxp1, Meis2), striosome markers (Bach2, Kcnip1, Khdrbs3, Nnat, Oprm1, Pbx3, Rasgrp1, Tshz1), matrix markers (Calb1, Cdh7, Epha4, Gda, Rasgrp2, Kcnq3, Penk, Sema3e, Stxbp6, Zfhx3), and D1/D2 pathway markers (Drd1, Ebf1, Sema5b, Tac1 for D1; Zfp503, Drd2, Oprd1, Penk, Adora2a, Six3, Gucy1a1 for D2). Clusters with high Dlx1 expression were interpreted as immature MSNs.

All figures and UMAP visualizations were generated and formatted using the scCustomize package (Marsh et al., 2023).

2.14. Neurobehavioral Test

2.14.1. Rotarod Test

The rotarod test (Model 47600; UGO Basile, Comerio, VA, Italy) was employed to evaluate motor coordination and balance in mice under both constant speed (12 rpm) and accelerating speed (4–40 rpm) conditions (Fig. 4a). For each trial, the latency to fall from the rotating rod was measured twice. If the difference between the two latency values exceeded 20 seconds, a third measurement was taken. Each trial was capped at a maximum duration of 300 seconds.

2.14.2. Grip Strength Test

Grip strength testing was conducted to assess forelimb muscle strength in mice. Each mouse was allowed to grasp a triangular metal bar attached to a force transducer using its forepaws, while the evaluator gently pulled the animal backward by the tail until it released its grip (Fig. 4b). The peak force (in gram force, gf) was recorded at the moment of release using a grip strength meter (#47200, Ugo Basile, Italy). For each mouse, five trials were performed, and the average of the three highest values—including measurements from the right, left, and both forelimbs—was calculated and normalized to body weight (gf/g).

2.14.3. Clasping Test

To evaluate hindlimb clasping behavior, mice were suspended by the tail for 10 seconds, and hindlimb posture was observed (Fig. 4c). The severity of clasping was scored based on the duration and extent of hindlimb retraction toward the body as follows:

- Score 0: Hindlimbs were fully extended with no clasping observed.
- Score 1: Hindlimbs were partially retracted for less than 5 seconds.
- Score 2: Hindlimbs were persistently clasped for 5 seconds or more, or forelimb clasping was also observed.

The test was performed in triplicate, and the average score was calculated for each mouse.

Figure 4. Behavioral assessment in R6/2 mouse model (a) Rota-rod test. (b) Grip strength test. (c) Clasping test.

2.15. Ethics Statement

All experimental procedures were reviewed and approved by the Institutional Animal Care and Use Committee (IACUC) of the Yonsei University Health System (approval numbers: 2022-0205, 2024-0611) and were conducted in accordance with the guidelines of the Association for Assessment and Accreditation of Laboratory Animal Care (AAALAC). The study complied with the 8th edition of the National Institutes of Health (NIH) Guide for the Care and Use of Laboratory Animals (NRC, 2011), the Animal Protection Act (2008), and the Laboratory Animal Act (2008).

All animals were housed under a 12-hour light/dark cycle with free access to food and water. At the end of the experiments, animals were euthanized via transcardial perfusion under anesthesia. Anesthesia was induced with a mixture of ketamine (100 mg/kg; Huons, Gyeonggi-do, Korea) and Rompun (10 mg/kg; Bayer Korea, Seoul, Korea) in a 10:1 ratio. Every effort was made to minimize animal suffering and distress throughout the experimental procedures.

2.16. Statistical Analysis

All data are presented as mean ± standard error of the mean (SEM). Each experiment was independently repeated at least three times, with three technical replicates per group. Statistical analyses were performed using SPSS Statistics version 27.0 (IBM Corp., Armonk, NY, USA), and all graphs were generated using GraphPad Prism version 9.

One-way analysis of variance (ANOVA) followed by Bonferroni post hoc test was used to assess differences between groups. For behavioral assessments including the rotarod test, clasping test, and body weight measurements, two-way repeated-measures ANOVA was conducted to evaluate interaction effects between time and treatment group. Statistical significance was defined as follows: $*p < 0.05$, $**p < 0.01$, $***p < 0.001$ (Bonferroni correction).

Table 1. Primers sequence for PCR

Genes	Primer Type	Sequence
Ascl1	Forward	5'- CGGAACTGATGCGCTGCAAACG -3'
	Reverse	5'- GGCAAAACCCAGGTTGACCAAC -3'
NeuroD1	Forward	5'- TTGCTACTCCAAGACCCAGAAA -3'
	Reverse	5'- GCAAGAAAGTCCGAGGGTTG -3'
GFAP	Forward	5'- TTGCTGGAGGGCGAAGAAAA -3'
	Reverse	5'- CATCCCGCATCTCCACAGTC -3'
C3	Forward	5'- GAG CGA AGA GAC CAT CGT ACT -3'
	Reverse	5'- TCT TTA GGA AGT CTT GCA CAG TG -3'
NeuN	Forward	5'- GAAACCGCAAGCCCTCATTTC -3'
	Reverse	5'- TTGGATGCCTCTTGGTTTGGT -3'
β-Tubulin	Forward	5'- TAGACCCCAGCGGCAACTAT -3'
	Reverse	5'- GTTCCAGGTTCCAAGTCCACC -3'
PPP1r1b	Forward	5'- AGATTCAGTTCTCTGTGCCCG -3'
	Reverse	5'- TGGGTCTCTTCGACTTTGGG -3'
GAD67	Forward	5'- CAAGTTCTGGCTGATGTGGA -3'
	Reverse	5'- GCCACCCTGTGTAGCTTTTC -3'

Foxp2	Forward	5'- CTGGAAAGCAAGCGAAAGAG -3'
	Reverse	5'- GAATGGAGATGAGTCCCTGA -3'
Meis2	Forward	5'- GACCACGATGATGCAACC -3'
	Reverse	5'- CCTGTGTCTTGCGCTAACTG -3'
Pbx3	Forward	5'- ATTACAGAGCCAAATTGACCCAG -3'
	Reverse	5'- TCTCGGAGAAGGTTCATCACAT -3'
Tshz1	Forward	5'- GCTGCTGCTGCTGCTGCTGCTG -3'
	Reverse	5'- AGAGAGAGAGAGAGAGAGAGAG -3'
Kcnip1	Forward	5'- CGACCCTCCAAAGATAAGATTG -3'
	Reverse	5'- AGTTCCTCTCAGCAAAATCGAC -3'
Orpm1	Forward	5'- GATCCTCTCTTCTGCCATTGGTC -3'
	Reverse	5'- TGAGCAGGTTCTCCCAGTACCA -3'
Bach	Forward	5'- TGAGGTACCCACAGACACCA -3'
	Reverse	5'- TGCCAGGACTGTCTTCACTG -3'
Kcnq3	Forward	5'- CAAGTACAGGCGCATCCAAAC -3'
	Reverse	5'- GGCCAGAATCAAGCATCCCA -3'
Penk	Forward	5'- TTCAGCAGATCGGAGGAGTTG -3'
	Reverse	5'- GAAGCGAACGGAGGAGAGAT -3'
Epha4	Forward	5'- AGTGATGTCGTACGGGGAGA -3'
	Reverse	5'- ACAAGGCAGTGTTAGGTCTGG -3'
Calb1 (Calbindin-1)	Forward	5'- CTTGCTGCTCTTTCGATGCCAG -3'
	Reverse	5'- GTTCCTCGGTTTCGATGAAGCC -3'
RasGRP2	Forward	5'- TCCCGGAAGGACAACTCCAAT -3'
	Reverse	5'- GGTTCAAGTCGAACTCTGCTG -3'
GAPDH	Forward	5'-GTGGAGCCAAAAGGGTCATCA-3'
	Reverse	5'-CCCTTCCACAATGCCAAAGTT-3'

3. RESULTS

Part1. Ascl1 study: Ascl1 reprograms astrocytes into immature GABAergic MSNs via a radial glia-like intermediate

1. Ascl1 Induces Astrocyte-to-Neuron Conversion Under Pathological Conditions

To assess the potential of astrocyte-to-neuron conversion under pathological conditions, primary astrocytes were treated with quinolinic acid (QA) to induce a reactive state. GFAP and C3 were significantly upregulated after QA treatment but were downregulated upon Ascl1 transduction, indicating a suppression of astrocyte reactivity and a possible transition toward a neuronal fate (Fig. 5). This concurrent reduction might reflect a pre-neuronal intermediate state, which represents a key transitional step in the conversion process. Further, the C3/GFAP ratio decreased in the Ascl1 group, thereby indicating the alleviation of the pathological reactive phenotype. To assess whether this shift corresponded to neuronal reprogramming, GABA expression was analyzed *in vitro* (Fig. 6). The number of $GFAP^+/GABA^+$ double-positive cells significantly increased in the Ascl1-treated group, indicating partial reprogramming (Fig. 6d). Moreover, the proportion of $GFAP^-/GABA^+$ cells also increased (Fig. 6e), indicating the loss of astrocytic identity and emergence of GABAergic neuronal features.

Finally, gene expression analysis using quantitative reverse transcription-polymerase chain reaction (qRT-PCR) validated this conversion at the transcriptional level (Fig. 7). Ascl1 treatment reduced the levels of astrocytic marker GFAP while increasing the levels of neuronal markers, such as β-tubulin, and GABAergic markers, including GAD67 and PPP1r1b. These results indicated that Ascl1 induces the GABAergic fate of reactive astrocytes *in vitro*.

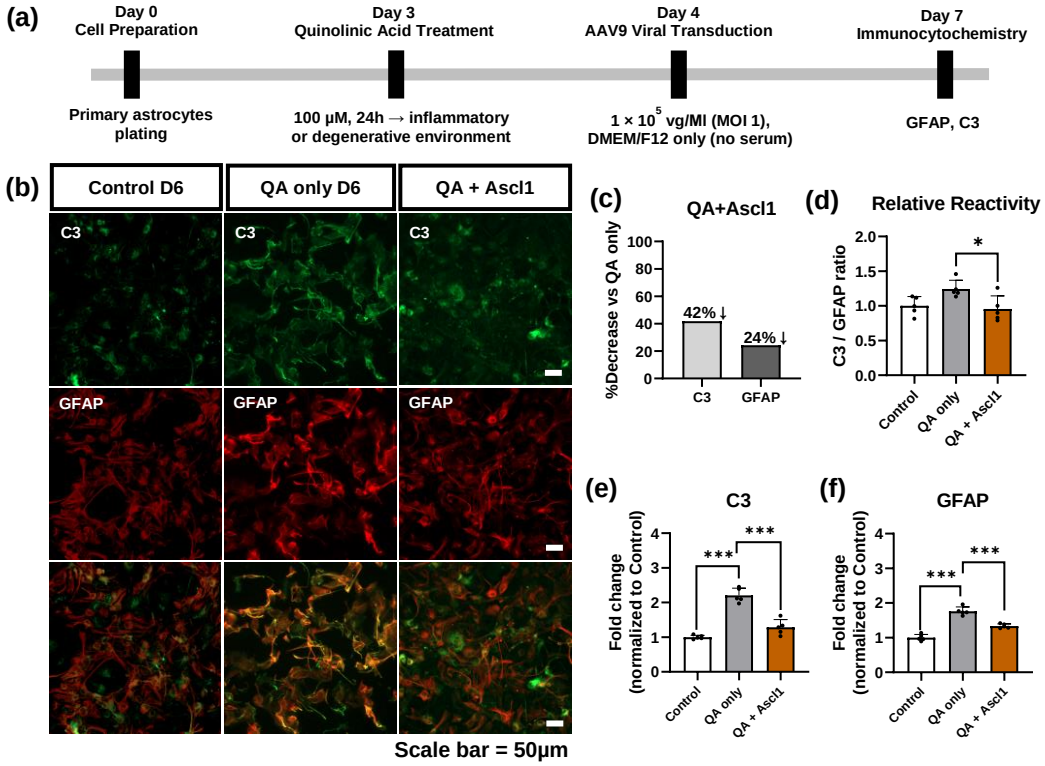

Figure 5. Ascl1-induced reduction in the levels of reactive astrocyte markers and promotion of transition toward a less reactive state

(a) Experimental timeline: Primary astrocytes were plated on day 0, treated with 100 μM QA for 24 h on day 3 to induce an inflammatory or degenerative state, transduced with AAV9-Ascl1 or control virus on day 4, and analyzed via immunocytochemistry on day 7. (b) Representative immunofluorescence images of C3 (green) and GFAP (red) in control, QA-only, and QA + Ascl1 groups. (c) Percent decrease in C3 and GFAP expression levels in the QA + Ascl1 group relative to the QA-only group. (d) Relative astrocyte reactivity is represented as the C3/GFAP fluorescence ratio. (e, f) Fold change in C3 and GFAP expression levels normalized to the control. Scale bar = 50 μm.

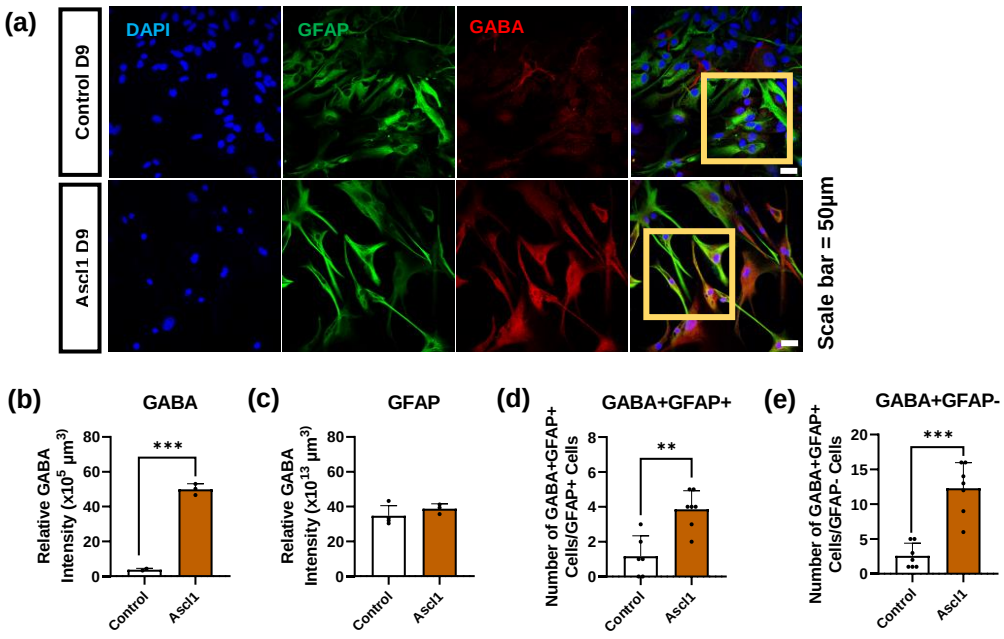

Figure 6. GABAergic neuronal conversion of astrocytes after Ascl1 treatment

Ascl1 significantly increased the number of $GABA^+$ cells derived from astrocytes. (a) Triple immunostaining for DAPI, GFAP, and GABA. (b-e) Quantification of $GABA^+$ cells, $GFAP^+$ cells, $GFAP^+/GABA^+$ double-positive cells, and $GFAP^-/GABA^+$ cells. Scale bar = 50 μm.

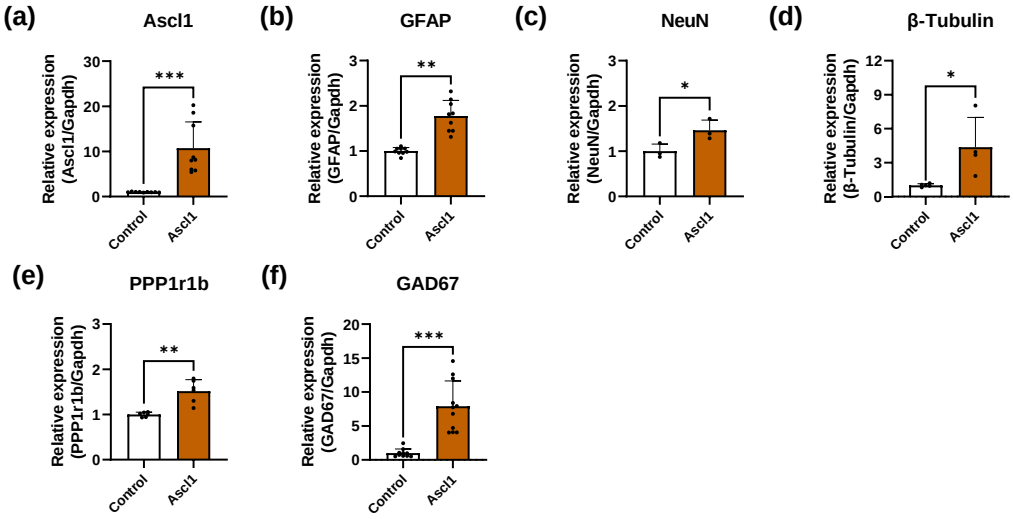

Figure 7. Ascl1-induced changes in the expression of genes associated with astrocyte-to-neuron conversion

Gene expression alters during Ascl1-induced astrocyte-to-neuron conversion. mRNA levels of (a) *Ascl1*, (b) *GFAP*, (c) *Neurod1*, (d) *β-tubulin*, (e) *PPP1r1b*, and (f) *GAD67*.

2. Ascl1 Promotes GABAergic Reprogramming in the Striatum *In Vivo*

Immunohistochemical, transcriptional, and lineage-tracing analyses were conducted in the striatum to assess the *in vivo* effects of Ascl1 on astrocyte-to-neuron reprogramming. At 4 and 8 weeks postinjection (wpi), immunostaining for GFAP, DARPP32, and GABA revealed time-dependent changes in the expression of these markers. GFAP intensity progressively decreased over time in the Ascl1-treated group (Fig. 8b), with a more pronounced reduction at 8 wpi. In contrast, $DARPP32^+$ and $GABA^+$ cell densities significantly increased over time (Fig. 8c–f), indicating that Ascl1 suppresses astrocytic identity while promoting the accumulation of striatal GABAergic neurons.

qRT-PCR was performed on striatal tissues to validate these phenotypic changes at the molecular level. Compared to the control group, the Ascl1 group demonstrated a significant reduction in GFAP expression at both 4 and 8 wpi, whereas neuronal genes, such as *β-tubulin* and *NeuN*, were significantly upregulated, particularly at 8 wpi (Fig. 9b–d). Furthermore, the striatal marker PPP1r1b and the GABAergic marker GAD67 were progressively upregulated over time (Fig. 9e–g), indicating a progressive transcriptional reprogramming toward GABAergic neuronal fate.

To identify whether these newly generated neurons arose from proliferative precursors, BrdU incorporation and co-staining were conducted for neuronal markers at 8 wpi. Double immunostaining demonstrated significantly increased numbers of $NeuN^+/BrdU^+$ and $DARPP32^+/BrdU^+$ cells in the Ascl1-treated group (Fig. 10a–f), indicating that a subset of neurons was derived from dividing astrocyte-like cells, potentially through a radial glia-like intermediate.

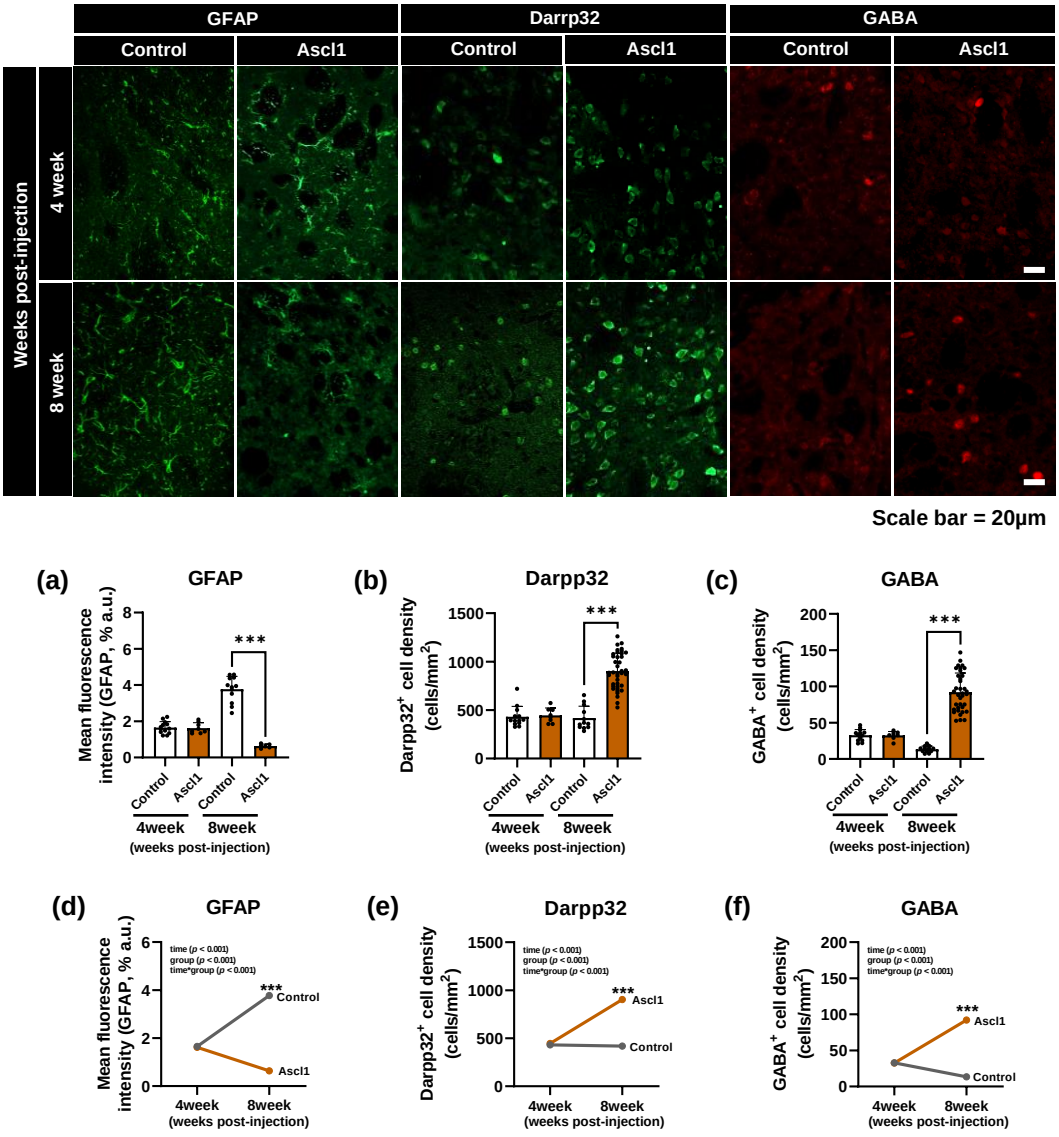

Figure 8. Downregulation of GFAP and upregulation of GABA and DARPP32 *in vivo* after Ascl1 treatment

Representative immunostaining images of GFAP (a), DARPP32 (b), and GABA (c) at 4 and 8 weeks postinjection (wpi). (a) Quantification of mean GFAP fluorescence intensity demonstrated its gradual decrease in the Ascl1 group. (d) Time-course analysis of GFAP

intensity revealed a marked GFAP reduction over time in the Ascl1 group compared to the control group. (b) DARPP32^{+} cell density increased upon Ascl1 treatment, and (e) a time-dependent comparison revealed a significant elevation at 8 wpi. (c) GABA^{+} cell density significantly increased after Ascl1 treatment, and (f) a time-course analysis revealed a progressive accumulation of GABAergic neurons over time. Scale bar = 20 μm.

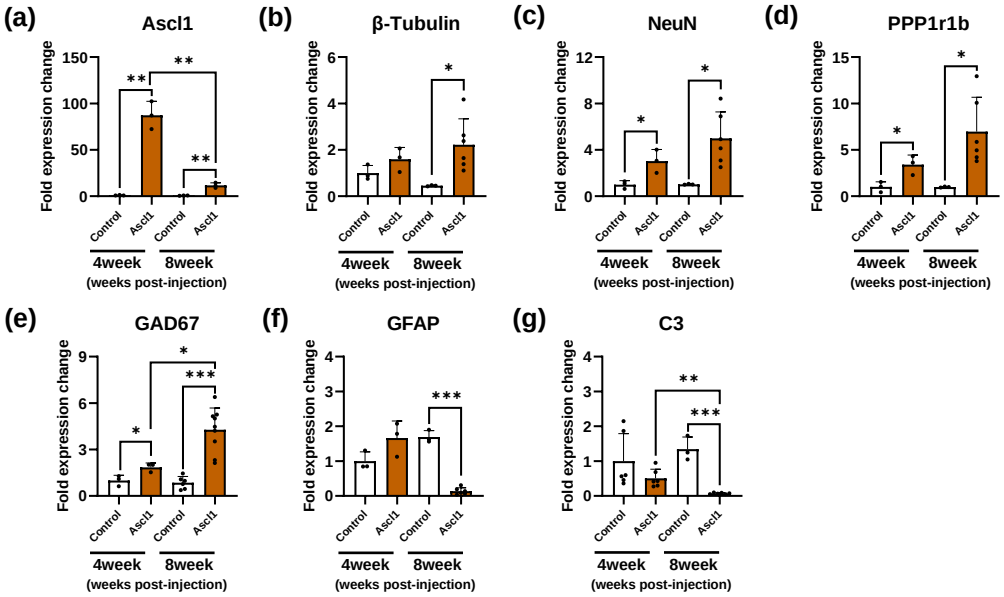

Figure 9. Gene expression changes over time in the striatum after Ascl1 treatment

Gene expression was analyzed with quantitative reverse transcription polymerase chain reaction (qRT-PCR) in striatal tissue at 4 and 8 wpi. (a) *Ascl1* expression was confirmed to be significantly upregulated in the treatment group. (b) Astrocytic marker *GFAP* was significantly downregulated at both time points. (c–d) Neuronal markers, *β-tubulin* and *NeuN*, were significantly upregulated, particularly at 8 wpi. (e–f) The striatal MSN marker PPP1r1b and GABAergic gene *GAD67* exhibited a consistent upregulation over time after Ascl1 treatment. Data are presented as mean ± standard error of the mean (SEM). *p < 0.05, **p < 0.01, ***p < 0.001.

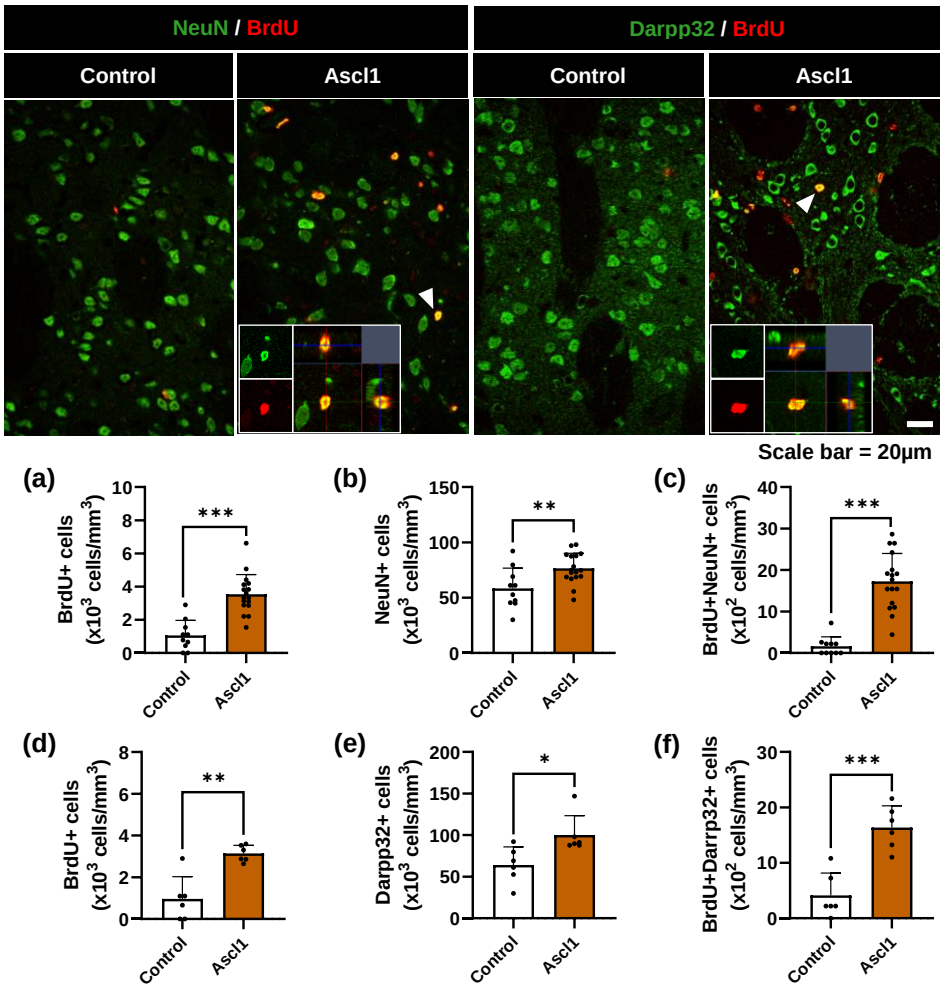

Figure 10. BrdU-based validation of the proliferative origin of Ascl1-induced neurons

(a) Double immunostaining of NeuN/BrdU and DARPP32/BrdU was performed at 8 wpi to trace the origin of reprogrammed neurons. (b) The number of $BrdU^+/NeuN^+$ cells significantly increased in the Ascl1 group, along with (c) an increase in $NeuN^+$ cell density. (d) Increased $BrdU^+$ cell count. (e) The number of $BrdU^+/DARPP32^+$ cells and (f) the proportion of $DARPP32^+$ cells among $DARPP32^+$ and $BrdU^+$ cells were significantly increased, indicating that a subset of reprogrammed neurons originated from proliferative precursor cells. Scale bar = 20 μm.

3. Clustering and Stepwise Differentiation of GABAergic Neurons Induced by Ascl1

GABAergic Neuron Subtype Analysis and Progressive Lineage Specification

To investigate the subtype diversity of reprogrammed neurons after Ascl1 overexpression, all GABAergic lineage cells were extracted and re-clustered across different conditions. UMAP-based clustering demonstrated 20 distinct GABAergic subclusters (clusters 0–19) (Fig. 11a). Most cells in the control group were confined to glial or immature clusters, such as clusters 0, 1, 2, and 10, with minimal representation of mature neuronal populations (Fig. 11b). In contrast, the Ascl1-treated group demonstrated a marked emergence and expansion of multiple distinct neuronal clusters, particularly clusters 4, 5, 6, and 8, which were highlighted as Ascl1-enriched populations (Fig. 11c). Quantitative comparison using donut plots further validated these differences. Clusters 4 and 5 were substantially increased in the Ascl1 group, whereas cluster 10, which was predominantly observed in the control group, was significantly decreased in the Ascl1 group (Fig. 11d). These results indicated that Ascl1 drives lineage progression from reactive astrocytes toward GABAergic neuronal fates by inducing distinct transcriptional states.

To further identify the molecular trajectory underlying Ascl1-induced neuronal reprogramming, the expression of stage-specific markers across the identified GABAergic subclusters was analyzed. Violin plots revealed a clear stepwise differentiation pattern. Radial glia-like clusters demonstrated high Egfr expression, indicating a glial or progenitor-like state (Fig. 12a). Early GABAergic progenitor clusters demonstrated the enrichment of *Zeb2* and *Nfib*, genes associated with initial GABAergic lineage commitment (Fig. 12b). Intermediate states expressed immature neuronal markers, such as Dlx1 and Sox6 (Fig. 12c), whereas the most differentiated clusters were characterized by a high expression of mature GABAergic genes, including *Gad1*, *Map2*, *Foxp2*, and *Bcl11b* (Fig. 12d).

These findings showed that Ascl1 drives a stepwise lineage transition, guiding astrocytes through progenitor and immature stages toward mature GABAergic neuron identity. This structured trajectory indicated that Ascl1 reprogramming partially recapitulates key stages

of GABAergic neurogenesis and contributes to the recovery of neuronal subtype identity.

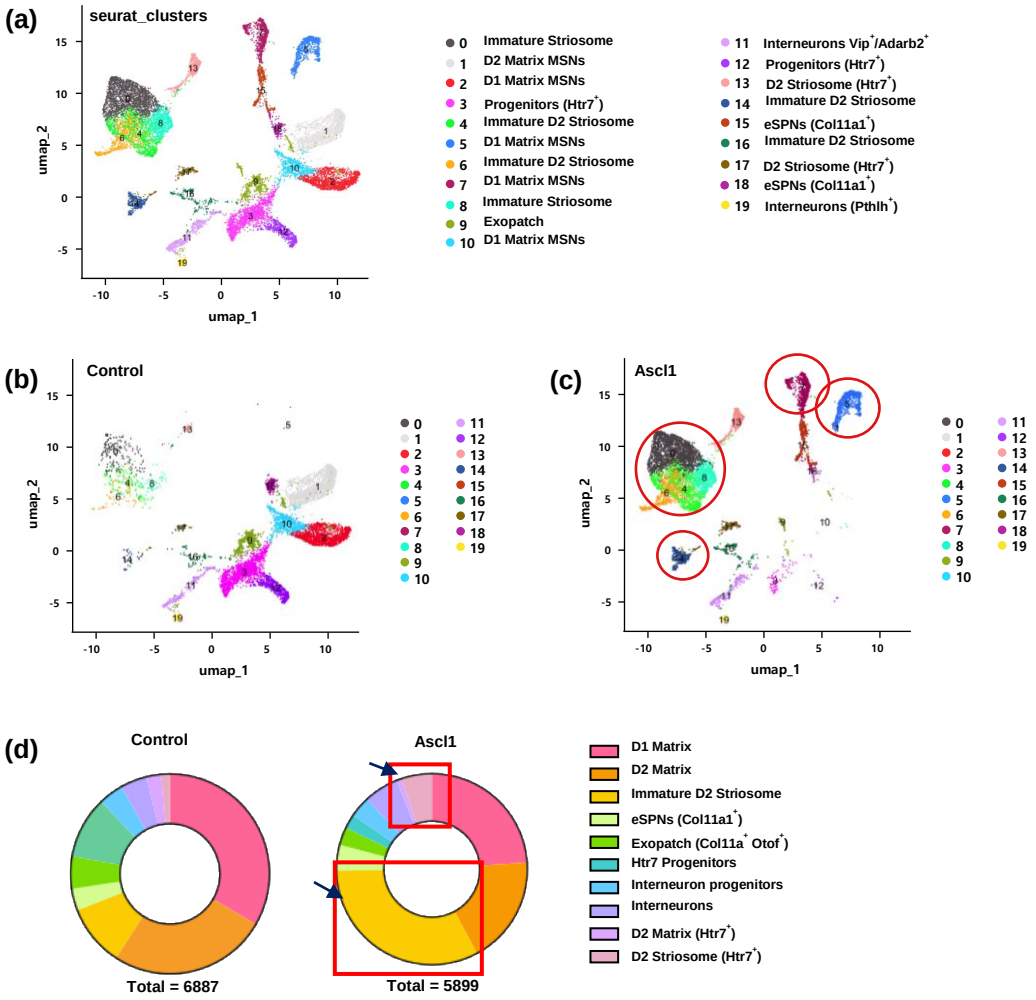

Figure 11. UMAP-based clustering of GABAergic neuron populations after Ascl1-induced reprogramming

(a) UMAP visualization of all GABAergic cells across different conditions, clustered using Seurat and annotated based on cluster identity (clusters 0–19). (b) Cluster distribution in the control group, demonstrating limited representation of neuronal clusters; most cells

remain in non-neuronal or immature states (e.g., clusters 0, 1, 2, 10). (c) Cluster distribution in the Ascl1 group reveals the emergence and expansion of distinct neuronal clusters (highlighted with red circles), including clusters 4, 5, 6, and 8, indicating Ascl1-mediated reprogramming into GABAergic neuronal fates. (d) Donut plots comparing cluster proportions between the control (left) and Ascl1 (right) groups. Blue and red arrows highlight cluster shifts associated with Ascl1 treatment. Notably, clusters 4 and 5 are substantially elevated in the Ascl1 group, whereas cluster 10 (control-dominant) is markedly reduced. Each cluster is color-coded and labeled (0–19) as shown beside the UMAPs.

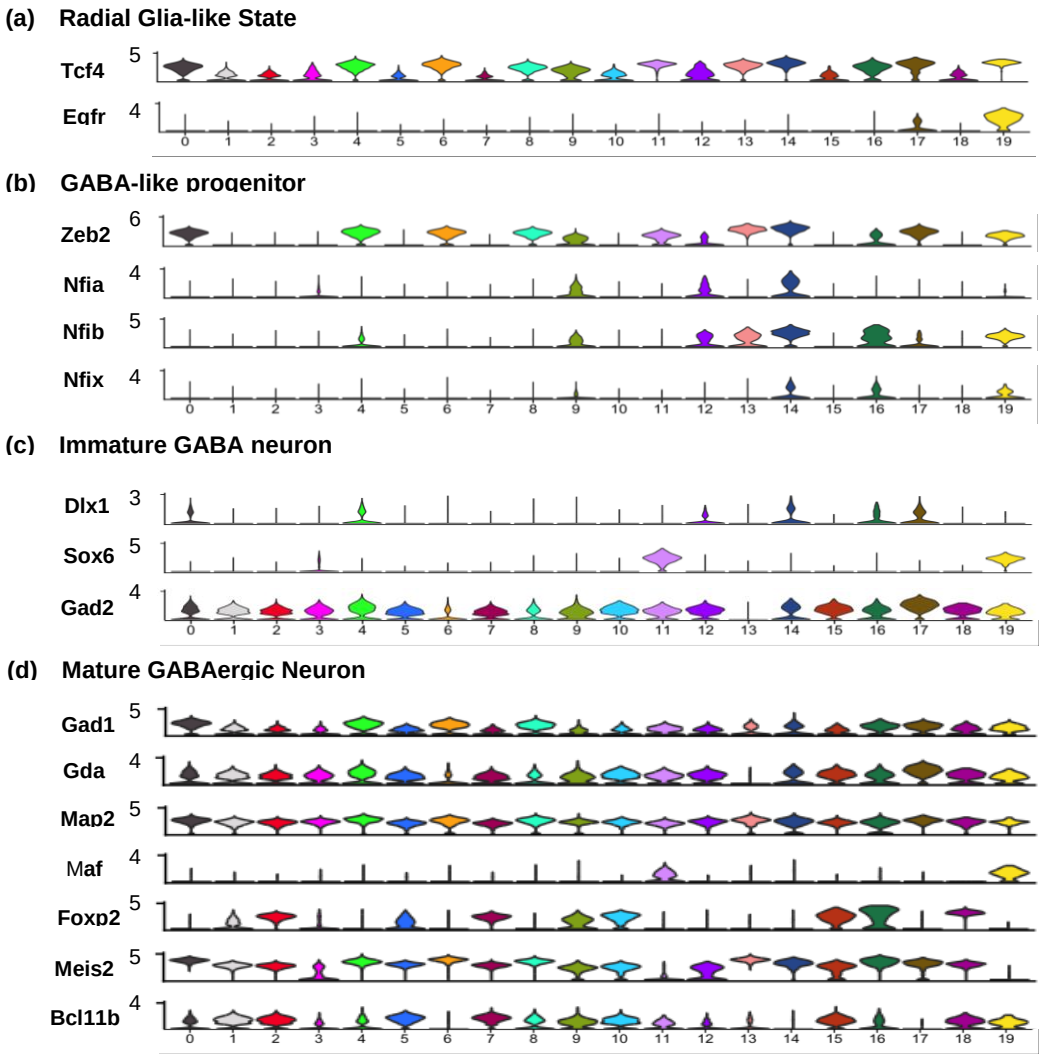

Figure 12. Progressive GABAergic lineage specification in Ascl1-induced clusters

(a–d) Violin plots illustrating the expression of lineage-specific markers across GABAergic subclusters: (a) Radial glia-like markers (e.g., Egfr), (b) GABAergic progenitor markers (e.g., Zic1 and Dlx1), (c) immature neuron markers (e.g., Dcx and Sox11), and (d) mature GABAergic markers (e.g., Gad1, Pvalb, and Slc32a1). These plots demonstrate stepwise differentiation toward mature GABAergic neuron identity in Ascl1-specific clusters.

4. Ascl1 Reprogramming Biases Fate Toward D2-Type MSNs

To identify the functional subtype of neurons induced by Ascl1, the expression of canonical markers for direct (D1-MSNs) and indirect pathway MSNs (D2-MSNs) was investigated. Violin plot analysis (Fig. 13a–c) revealed that Ascl1-enriched clusters—particularly clusters 12, 13, and 16—demonstrated an upregulation of D2-MSN markers, such as Drd2, Penk, Synpr, and Cartpt, whereas the expression of D1-associated genes, including *Drd1*, *Foxp1*, and *Dner*, remained relatively low. These results indicated that Ascl1-induced neurons predominantly acquire a D2-type MSN identity, with partial enrichment of striosome-associated features.

To further categorize the regional identity of the induced neurons, the expression of striosome and matrix compartment markers was investigated. Ascl1-enriched clusters displayed strong expression of striosome-associated markers, including Oprm1, Pbx3, Meis2, Tac1, and Foxp2 (Fig. 15a). In contrast, matrix-specific genes, such as *Calb1*, *Epha4*, and *Rasgrp2*, were downregulated in these same clusters (Fig. 14b), indicating that Ascl1-driven reprogramming promotes not only D2 identity but also preferential acquisition of striosomal fate.

These results were further validated by qRT-PCR analysis of bulk striatal tissue. Ascl1-treated mice demonstrated a significant upregulation of striosome-related genes, such as *Foxp2*, *Meis2*, *Pbx3*, *Tac1*, and *Oprm1* (Figs. 15a–g). In contrast, the expression of matrix-associated markers, including Epha4, Calb1, and RasGRP2, either remained unchanged or significantly decreased (Fig. 15h–l). Together, these data revealed that Ascl1 reprograms astrocytes into D2-type MSNs, which are considered crucial for restoring balance in the striatal circuitry in HD and other basal ganglia disorders.

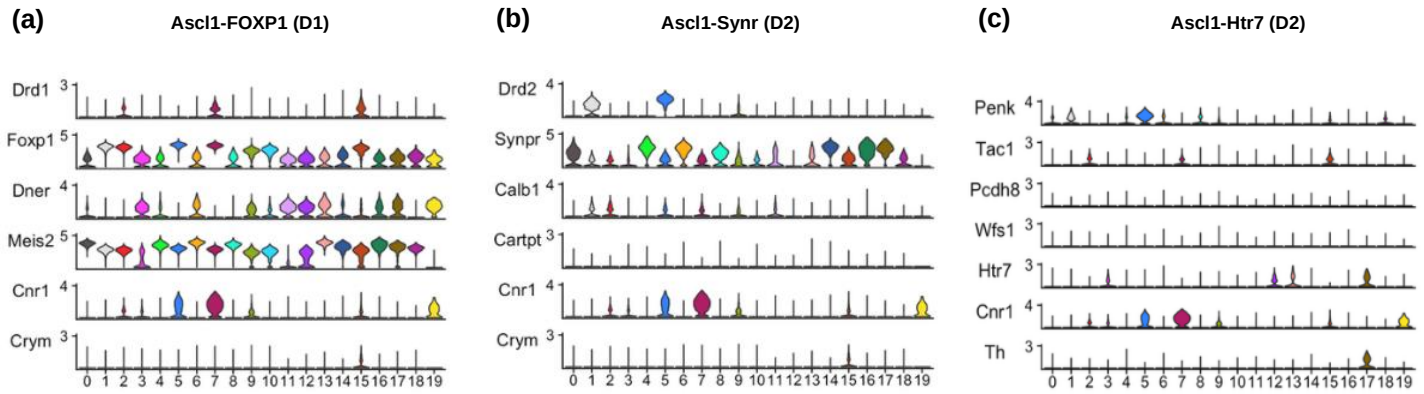

Figure 13. Expression of MSN subtype markers indicates D2 identity in Ascl1-induced clusters

(a) Violin plots illustrating the expression of direct pathway (D1-type MSN) markers, including Drd1, Foxp1, Dner, Meis2, Cnr1, and Crym. These markers were weakly expressed in Ascl1-induced clusters, except for Meis2, which demonstrated moderate expression.

(b) Indirect pathway (D2-type MSN) markers, such as Drd2, Synpr, Calb1, Cartpt, and Crym, were more prominently expressed, particularly in clusters 12, 13, and 16.

(c) Additional D2-associated or striosome-related genes, including *Penk*, *Tac1*, *Pcdh8*, *Wfs1*, *Htr7*, and *Th*, were upregulated in these clusters. These patterns indicate that Ascl1 treatment predominantly induces D2-type MSN identity with partial enrichment of striosomal characteristics.

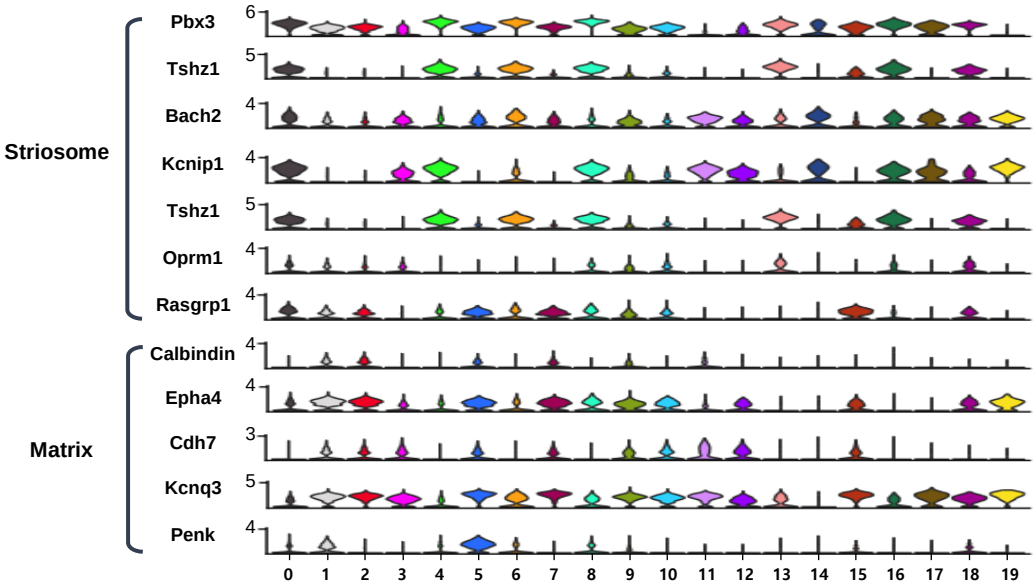

Figure 14. Cluster-specific expression of striosome- and matrix-associated markers in Ascl1-induced populations

(a) Violin plots illustrating upregulation of striosomal markers, including Oprm1, Pbx3, Tac1, Foxp2, Meis2, Ebf1, and Zfhx3, in clusters 12, 13, and 16. (b) Matrix-associated genes, such as *Calb1*, *Epha4*, *Cck*, *Kcnq4*, *Rasgrp1*, *Rasgrp2*, and *Sema3e*, were weakly expressed in the same clusters, indicating a striosome-like identity in Ascl1-induced neurons.

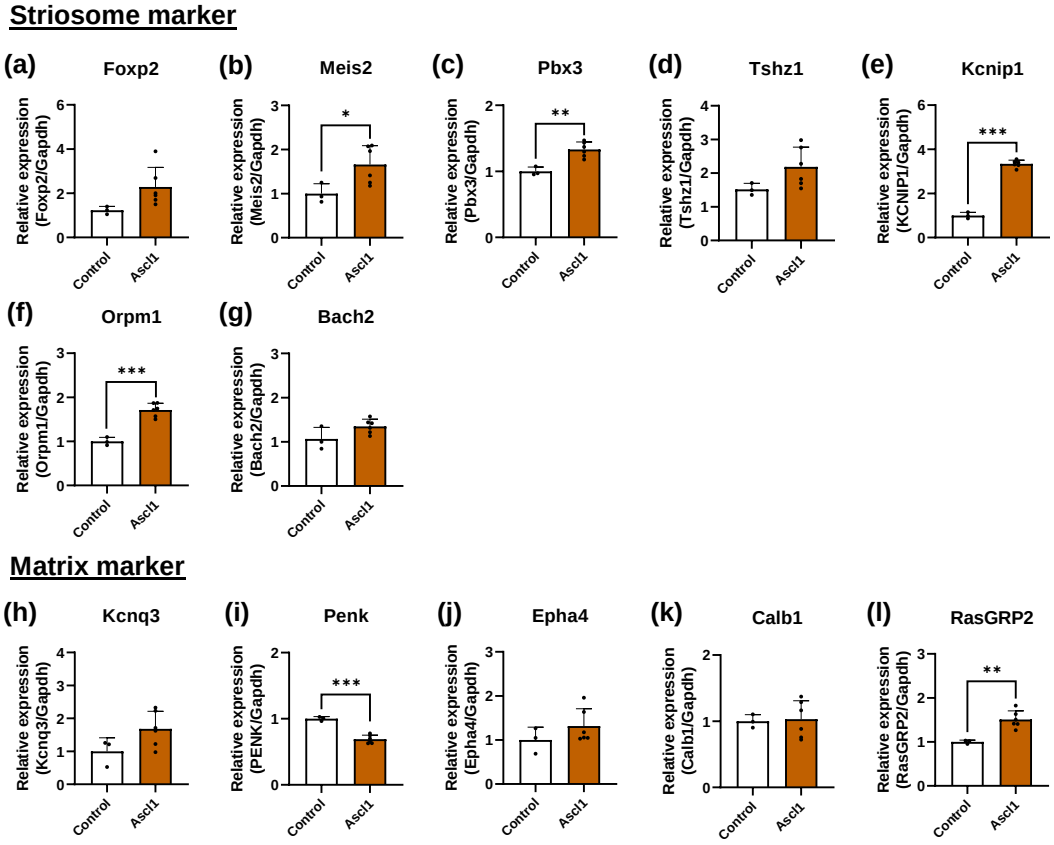

Figure 15. qRT-PCR validation of the expression of striosome- and matrix-associated markers in the striatum of Ascl1-treated mice

(a–g) Bulk qRT-PCR analysis revealed significant upregulation of striosomal markers, including Foxp2, Meis2, Pbx3, Tac1, Oprm1, Rasgrf1, and Penk, in the Ascl1 group. (h–l) In contrast, the expression of matrix-associated genes, such as *Epha4*, *Calb1*, and *RasGRP2*, decreased or remained unchanged, thereby indicating a preferential induction of striosomal fate *in vivo*.

5. Subtype-Specific Reprogramming for Striatal Circuit Restoration

To identify whether Ascl1-induced neuronal reprogramming results in functional recovery in the HD model, the expression of chloride cotransporters, KCC2 and NKCC1, which are crucial GABAergic signaling regulators, was first investigated. Western blot analysis revealed significant KCC2 downregulation in the HD group compared to the wild-type (WT) controls, but its expression was markedly restored in Ascl1-treated mice (Fig. 16a–b). In contrast, NKCC1 levels remained unchanged across all groups. Quantitative densitometry validated the selective upregulation of KCC2 (Fig. 16c) with no effects on NKCC1 (Fig. 16d). Consistent with these findings, single-cell RNA sequencing data demonstrated cluster-specific Slc12a5 (KCC2) enrichment in Ascl1-induced neuronal populations (Fig. 16e), whereas Slc12a2 (NKCC1) was not expressed in those clusters. These results indicated that Ascl1 promotes a restoration of inhibitory synaptic function via enhanced KCC2 expression, potentially normalizing the GABA reversal potential in reprogrammed neurons.

To assess the translation of these molecular changes into functional improvements, behavioral testing was performed. The rotarod test revealed that Ascl1-treated mice demonstrated significantly prolonged latency to fall compared to HD controls at both 4 and 8 wpi (Fig. 17a–d), indicating improved motor coordination and balance. Similarly, grip strength was significantly enhanced in the Ascl1 group, as shown by both longitudinal (Fig. 17e) and average force analyses (Fig. 17f). The clasping test revealed that Ascl1-treated group demonstrated reduced clasping scores and fewer clasping-positive mice compared to HD controls (Fig. 17g–h), reflecting attenuated motor deficits. Together, these findings indicated that Ascl1-mediated reprogramming not only restores molecular markers of functional GABAergic signaling but also results in measurable improvements in motor behavior.

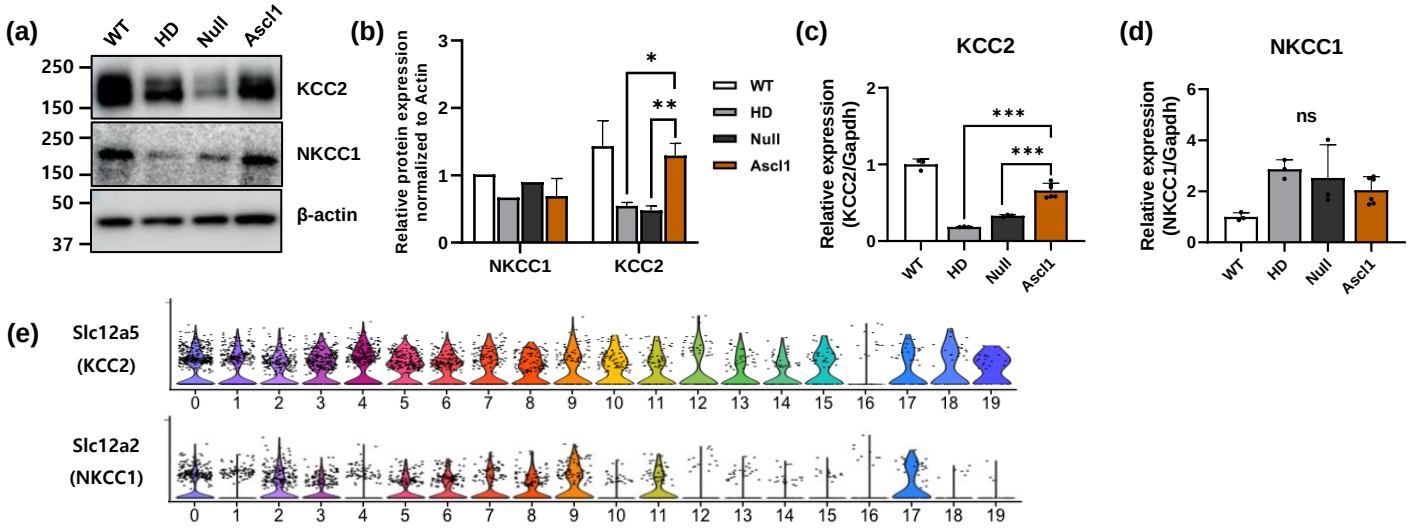

Figure 16. Restoration of KCC2 expression and GABAergic signaling after Ascl1 treatment

(a) Western blot analysis of KCC2 and NKCC1 from striatal tissue. (b) Quantification of band intensities demonstrates KCC2 downregulation in the HD group; however, its expression was significantly restored by Ascl1. In contrast, NKCC1 levels were unaffected. (c–d) Relative densitometric analysis of KCC2 and NKCC1. (e) Violin plots from single-cell RNA-sequencing (snRNA-seq) data illustrating cluster-specific enrichment of Slc12a5 (KCC2) in Ascl1-induced neuronal populations, whereas Slc12a2 (NKCC1) was absent. These results indicate functional recovery of GABA reversal potential mediated by Ascl1-induced reprogramming.

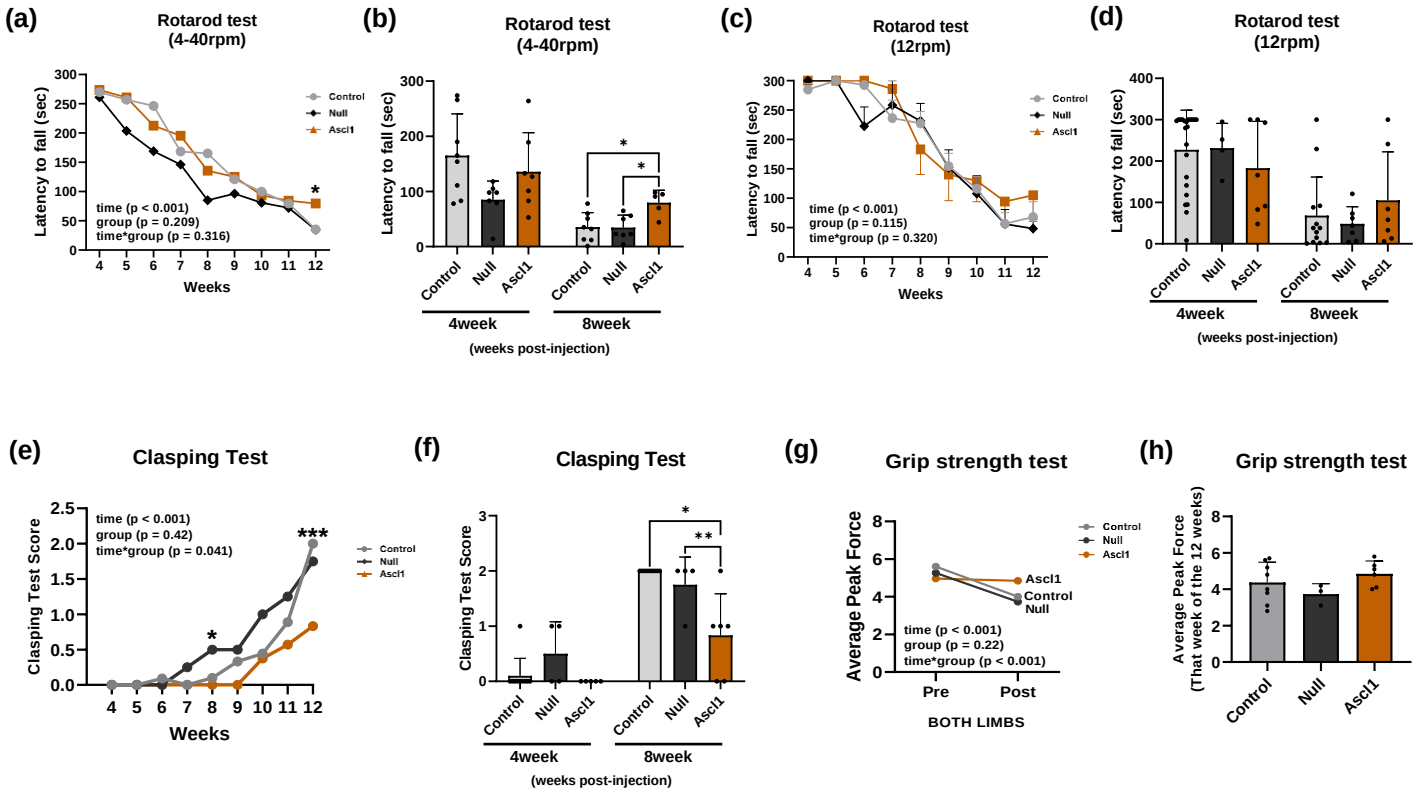

Figure 17. Ascl1 treatment improves motor coordination and reduces motor impairment in HD mice

(a–b) Rotarod test at 4 rpm revealed significantly prolonged latency to fall in the Ascl1 group compared to HD mice (null) across time points. This improvement was evident at both 4 and 8 wpi. (c–d) Motor performance at higher rotarod speed

(12 rpm) exhibited a time-dependent decline in the null group, whereas Ascl1-treated mice exhibited the same or improved performance, especially at 8 wpi. (e–f) Clasping behavior, which is a marker of motor dysfunction, progressively worsened in the null group but was significantly attenuated in the Ascl1 group, with reduced clasping scores and fewer clasping-positive mice. (g–h) Grip strength test revealed a trend toward improved or the same forelimb strength in Ascl1-treated mice at 12 wpi, with higher average peak force compared to the null group.

Part2. NeuroD1 study: NeuroD1 directly converts astrocytes into diverse types of GABAergic neurons, inducing a mixture of striosomal and matrix MSN subtypes

1. Direct Conversion of Reactive Astrocytes Into GABAergic Neurons by NeuroD1

To investigate the ability of NeuroD1 to directly convert reactive astrocytes into neurons under inflammatory conditions, a QA-induced reactive astrocyte model was employed, as described in Part 1. Primary astrocytes were treated with 100 μM QA to induce a pathological state and then transduced with AAV9-GFAP-NeuroD1. Immunocytochemistry analysis on day 7 revealed significant C3 and GFAP downregulation after NeuroD1 treatment (Fig. 18b–f). This finding was further validated by a decrease in the C3/GFAP ratio, indicating a reversal of astrocyte reactivity. Quantitative analysis revealed a marked reduction in fluorescence intensity and mRNA expression of both C3 and GFAP in the NeuroD1 group compared to QA-only controls. These results indicated that NeuroD1 mitigates the reactive features of astrocytes under pathological conditions and potentially initiates direct neuronal conversion without passing through a proliferative intermediate.

NeuroD1 treatment significantly increased the number of $GABA^+$ cells, but GFAP levels remained relatively unchanged, indicating a direct conversion mechanism without an intermediate progenitor phase (Fig. 19a–e). This result was further validated by the increase in the numbers of both $GABA^+/GFAP^+$ double-positive and $GFAP^-/GABA^+$ cells.

Consistently, RT-qPCR revealed an upregulation of neuronal and GABAergic markers, including NeuroD1, NeuN, β-tubulin, GAD67, and PPP1r1b, and a downregulation of GFAP (Fig. 20a–f). Together, these findings revealed that NeuroD1 mediates rapid and direct astrocyte-to-neuron conversion under pathological conditions.

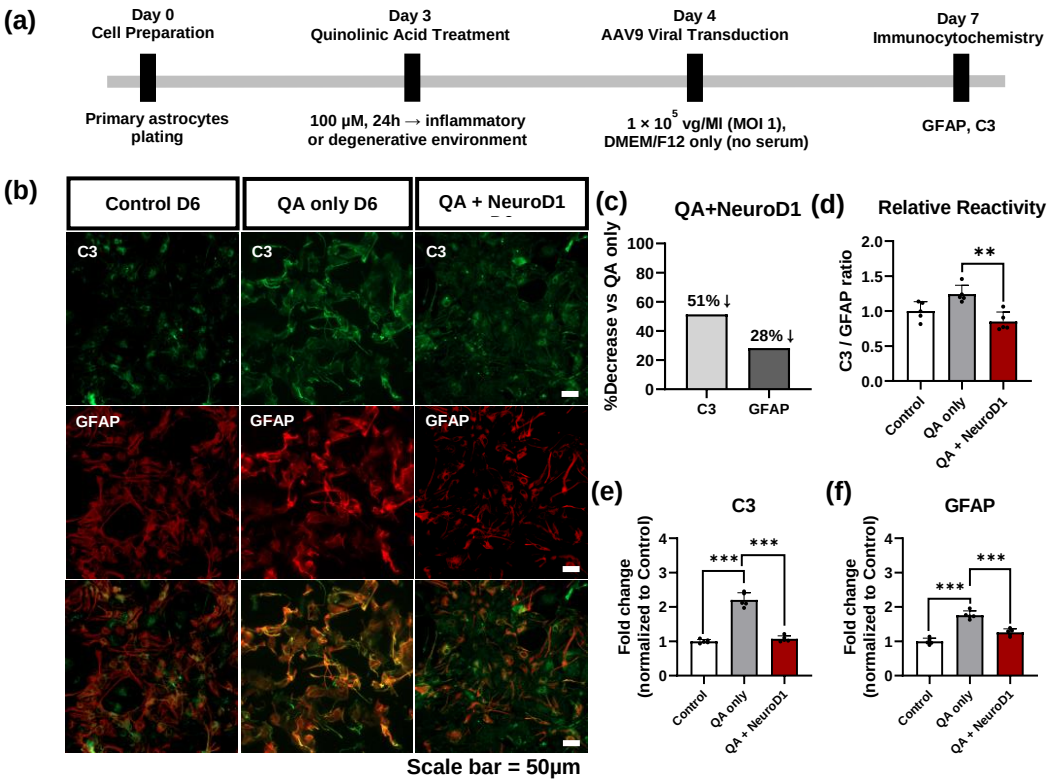

Figure 18. NeuroD1 treatment reduces the levels of reactive astrocyte markers under pathological conditions

In QA-induced reactive astrocytes, GFAP and C3 were significantly downregulated after NeuroD1 transduction. (a) Experimental timeline: Primary astrocytes were plated on day 0, treated with 100 μM QA on day 3 for 24 h to induce an inflammatory or degenerative environment, transduced with AAV9-NeuroD1 or control virus on day 4, and subjected to immunocytochemistry analysis on day 7. (b) Representative immunofluorescence images demonstrating C3 (green) and GFAP (red) in the control D6, QA only, and QA + NeuroD1 groups. (c) Percent decrease in average fluorescence intensities of C3 and GFAP in the QA + NeuroD1 group relative to the QA-only group. (d) Relative astrocyte reactivity evaluated by the C3/GFAP fluorescence ratio. (e, f) Fold change in C3 and GFAP expression levels normalized to the control.

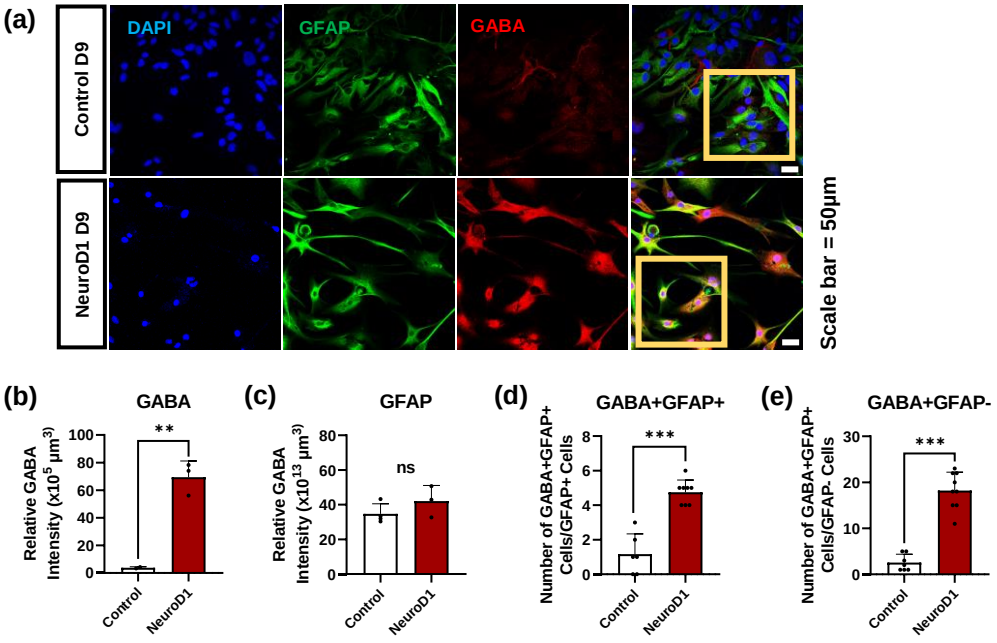

Figure 19. NeuroD1 promotes direct astrocyte-to-neuron conversion *in vitro*

(a) Triple immunofluorescence for DAPI, GFAP, and GABA. (b) $GABA^+$ cell quantification. (c) GFAP intensity did not change significantly. (d) Increase in the number of $GABA^+/GFAP^+$ double-positive cells. (e) Significant increase in $GFAP^-/GABA^+$ population. Scale bar = 50 μm.

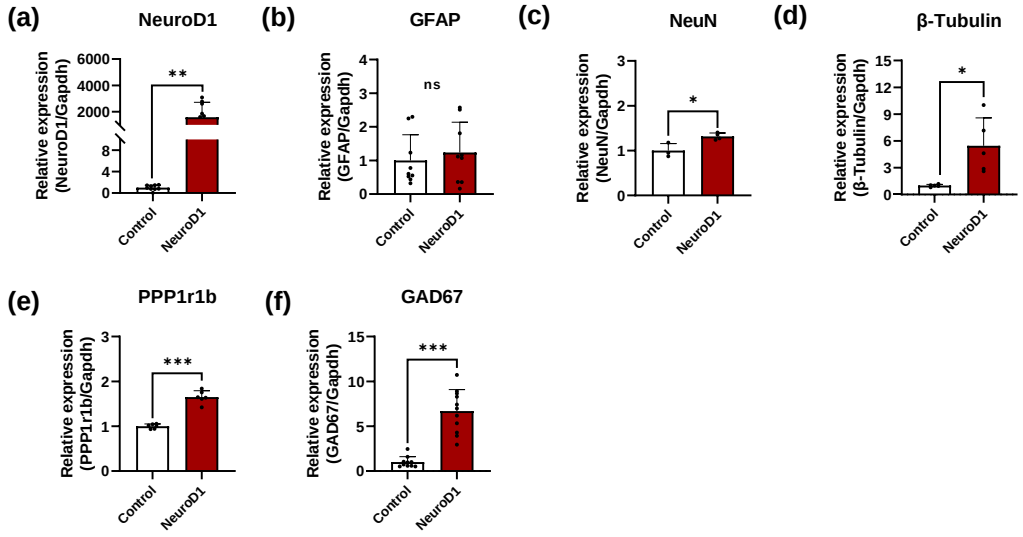

Figure 20. Gene expression changes after NeuroD1-mediated reprogramming

(a) NeuroD1 expression validation. (b) GFAP downregulation. (c–f) Upregulation of neuronal markers (NeuN and β-tubulin), striatal MSN marker PPP1r1b, and GABAergic gene *GAD67*, indicating functional neuronal conversion.

2. In Vivo Maturation of GABAergic Striatal Neurons From Astrocytes by NeuroD1

To assess the *in vivo* effect of NeuroD1, neuronal and astrocytic markers in the striatum at 4 and 8 wpi were investigated. Immunohistochemistry analysis revealed that GFAP expression decreased over time, whereas the density of $DARPP32^+$ and $GABA^+$ cells progressively increased in the NeuroD1 group compared to the control group (Fig. 21a–f). These changes indicated successful reprogramming and functional maturation of striatal neurons.

Consistently, qRT-PCR analysis of striatal tissue revealed significant upregulation of neuronal markers (β-tubulin and NeuN), striatal MSN-related gene (PPP1r1b), and the GABAergic marker GAD67 after NeuroD1 treatment, whereas astrocytic and reactive markers, such as GFAP and C3, were markedly downregulated (Fig. 22a–g). These results revealed that NeuroD1 induces *in vivo* astrocyte-to-neuron conversion and promotes the acquisition of GABAergic striatal neuron identity.

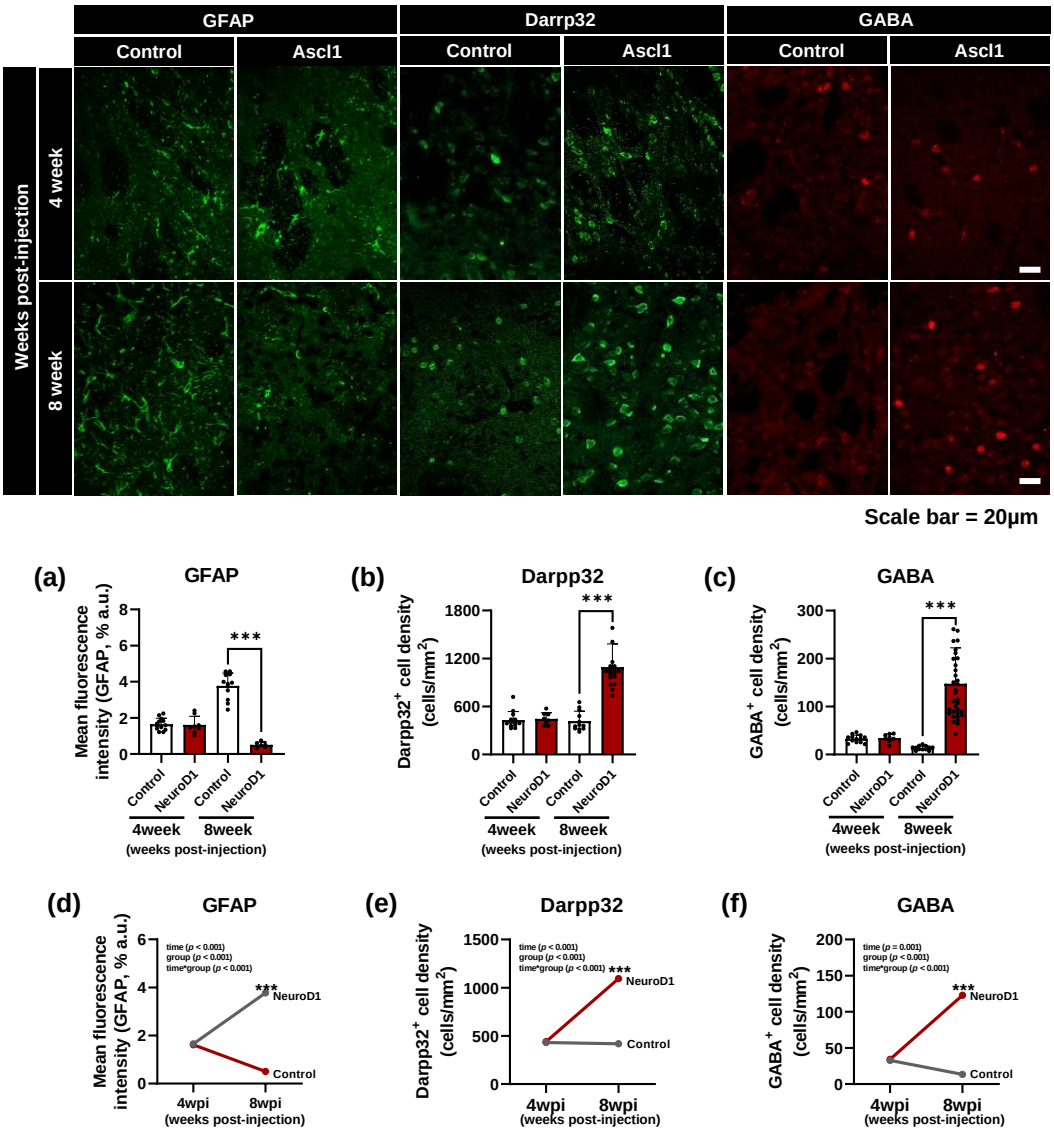

Figure 21. Time-dependent increase in GABAergic and DARPP32$^+$ neurons after NeuroD1 treatment *in vivo*

(a) Representative immunostaining images of GFAP and DARPP32 in control and NeuroD1-injected striatum at 4 and 8 wpi. (b) Quantification of GFAP intensity. (c)

Quantification of DARPP32^{+} cell density. (d) Time-course comparison of DARPP32^{+} cells. (e) Quantification of GABA^{+} cell density. (f) Time-course comparison of GABA^{+} cells. Scale bar = 20 μm.

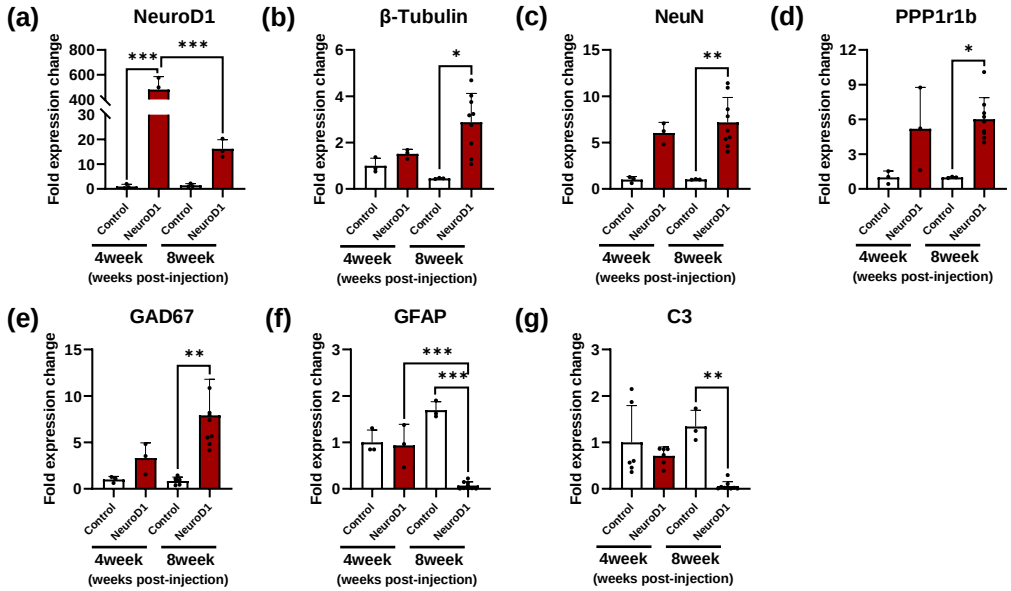

Figure 22. Gene expression changes in the striatum after *in vivo* NeuroD1 reprogramming

(a) NeuroD1 expression validation. (b–c) Upregulation of neuronal markers β-tubulin and NeuN. (d–e) Significant upregulation of MSN marker PPP1r1b and GABAergic marker GAD67. (f–g) Downregulation of astrocytic and reactive astrocyte markers GFAP and C3. Data are presented as mean ± SEM. *p < 0.05, **p < 0.01, ***p < 0.001.

3. NeuroD1 Induces GABAergic Neuron Reprogramming With Striatal D2-MSN-Like Identity

To characterize the cellular heterogeneity of GABAergic neurons generated by NeuroD1, unsupervised clustering and UMAP visualization of GABAergic cells were performed across all conditions (Fig. 23a). A total of 22 clusters (0–21) were identified. Most cells in the control group were enriched in non-neuronal or immature clusters (e.g., clusters 0, 1, 2, and 10), whereas the NeuroD1 group demonstrated the emergence and expansion of distinct neuronal clusters, including clusters 4, 5, 6, 8, 13, and 18 (Fig. 23b–c).

This shift in cellular composition was further confirmed by donut plot analysis, which demonstrated a marked increase in mature neuronal clusters and a reduction in immature populations after NeuroD1 treatment (Fig. 23d). Clusters 4, 5, and 6 were notably expanded in the NeuroD1 group, whereas clusters 0 and 1 were significantly reduced.

To further assess the maturation state of NeuroD1-induced GABAergic neurons, the expression patterns of both immature and mature neuronal markers were examined across identified clusters. Immature GABAergic markers, including Sox6, Dlx1, and Gad2, were broadly expressed across multiple clusters in the NeuroD1 group (Fig. 24a). These markers are typically associated with early-stage progenitors or incompletely differentiated GABAergic neurons, thereby indicating the presence of intermediate reprogramming states among the converted populations.

In contrast, mature GABAergic and striatal neuronal markers, such as Gad1, Gda, Map2, Foxp2, Meis2, Bcl11b, Zeb2, and Pam, were selectively enriched in specific clusters, particularly those expanded with NeuroD1 treatment (Fig. 24b). The expression of these markers indicates the acquisition of a more mature GABAergic phenotype and indicates differentiation toward MSN identity.

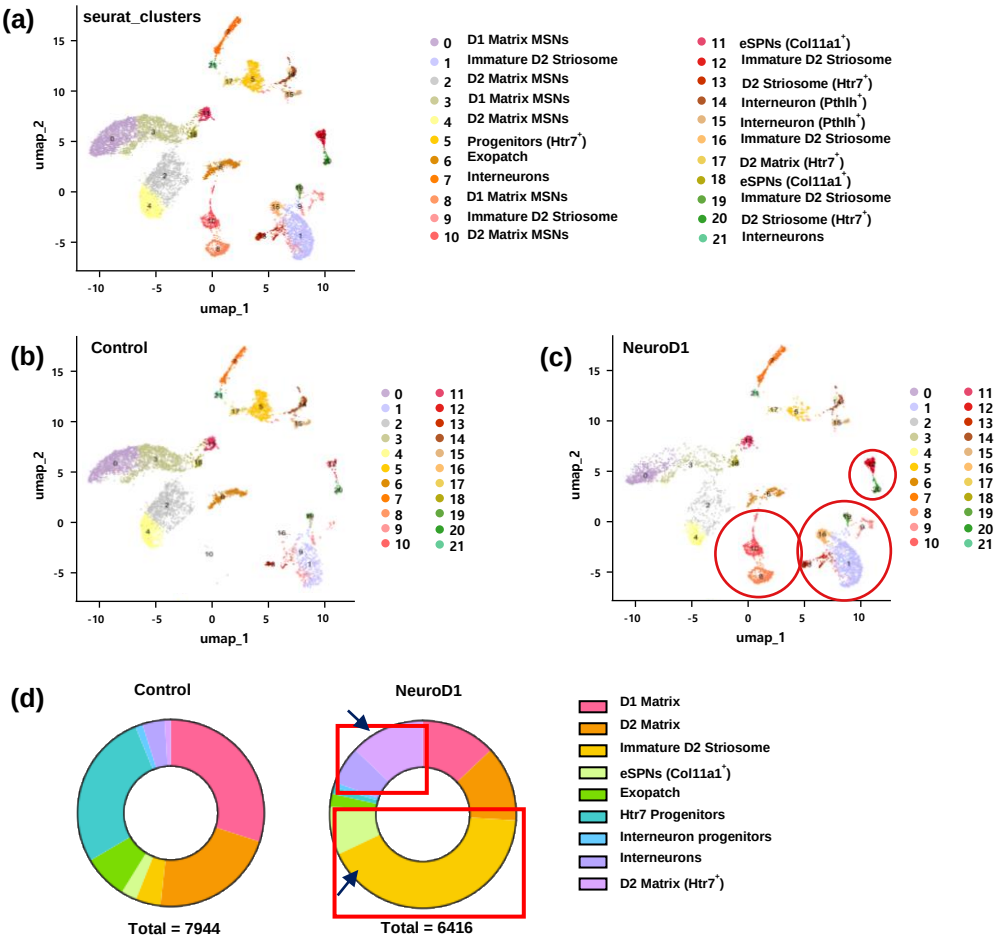

Figure 23. UMAP-based clustering and cluster composition analysis of NeuroD1-induced GABAergic populations

(a) UMAP visualization of all GABAergic cells across conditions, clustered using Seurat (clusters 0–21). (b) Cluster distribution in the control group indicates that most cells remain in non-neuronal or immature clusters (e.g., clusters 0, 1, 2, 10). (c) In contrast, the NeuroD1 group demonstrates the emergence and expansion of multiple neuronal clusters (highlighted with red circles), including clusters 4, 5, 6, 8, 13, and 18, indicating NeuroD1-induced reprogramming toward GABAergic neuronal fates. (d) Donut plots comparing

cluster proportions between the control and NeuroD1 groups. Red and blue arrows highlight increased representation of mature neuronal clusters (e.g., 4, 5, 6) and decreased immature clusters (e.g., 0, 1) in the NeuroD1 group.

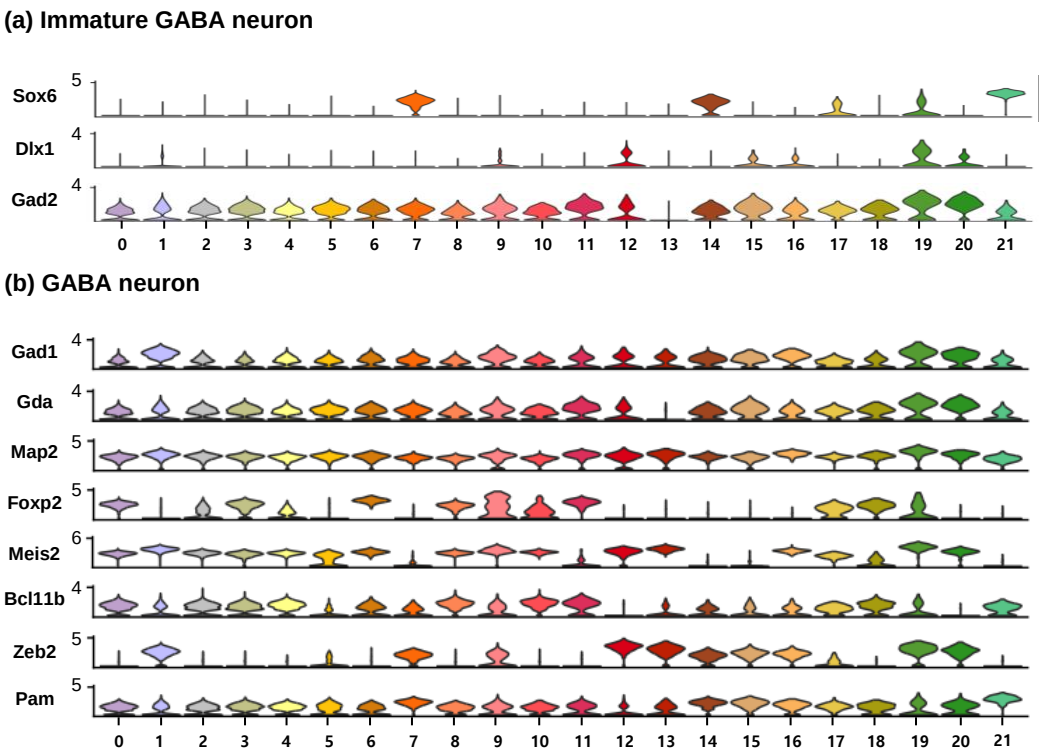

Figure 24. Gene expression in NeuroD1-enriched GABAergic clusters 13 and 20

(a) Violin plots of immature GABAergic markers (Sox6, Dlx1, and Gad2). (b) Expression of mature GABAergic striatal markers (Gad1, Gda, Map2, Foxp2, Meis2, Bcl11b, Zeb2, and Pam) in the same cluster.

4. *In Vivo* Transcriptomic and Molecular Validation of D2-Type Striosomal MSN Fate Determination by NeuroD1

To define the subtype and compartment identity of NeuroD1-induced striatal neurons, the expression of MSN pathway markers and striosome–matrix compartment genes across clusters 0–21 was analyzed.

Direct pathway markers (Drd1, Tac1, Isl1, and Ebf1) and indirect pathway markers (Drd2, Penk, Adora2a, and Sp9) were differentially enriched in distinct clusters (Fig. 25a–b), indicating the presence of both D1- and D2-type MSN populations. Compartment-related genes (*Ppp1r1b*, *Oprm1*, *Grik3*, and *Cnr1*) also demonstrated cluster-specific expression patterns (Fig. 25c). Figure 26 illustrates that striosome markers (Pbx3, Oprm1, Foxp2, Meis2, Bach2, Kcnip1, and Zfhx3) were enriched in specific clusters, whereas matrix markers (Calbindin, Epha4, Kcnq3, Sema3e, and Stxbp6) were expressed in separate clusters, indicating compartment-specific segregation at the transcriptomic level. Post hoc gene expression analysis in NeuroD1-injected striatal tissue validated the upregulation of striosome markers (Foxp2, Meis2, Pbx3, Tac1, Kcnip1, Oprm1, and Bach2) with little or no change in matrix markers (Kcnq4, Penk, Epha4, Calb1, and RasGRP2; Fig. 27).

These results indicated that NeuroD1-induced neurons demonstrate both MSN subtype diversity and compartmental identity consistent with striosomal and matrix features.

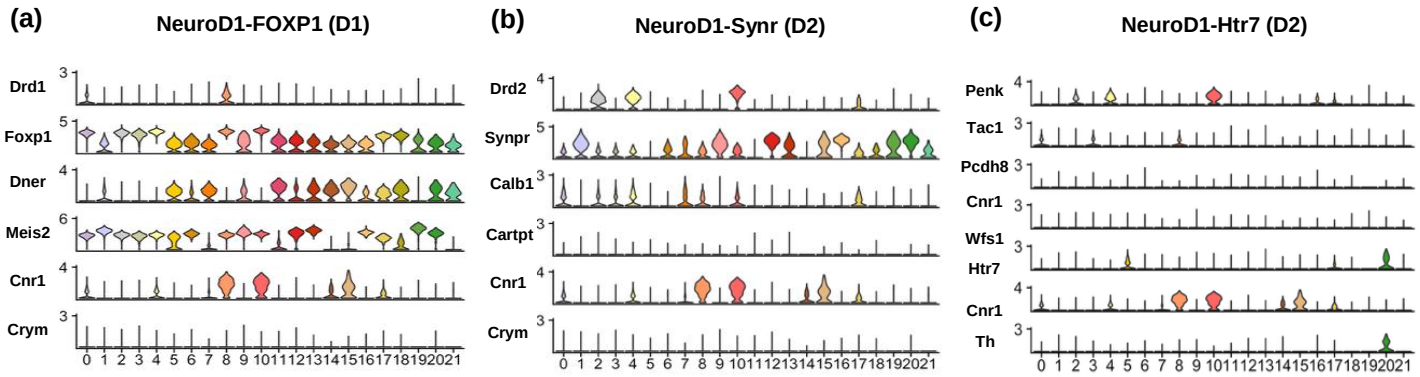

Figure 25. Violin plots of striatal MSN subtype markers across clusters

Expression of MSN-related markers across clusters 0–21 in NeuroD1-treated GABAergic populations. (a) Direct pathway–related markers: Drd1, Tac1, Isl1, and Ebf1. (b) Indirect pathway–related markers: Drd2, Penk, Adora2a, and Sp9. (c) Striosome–matrix compartment markers: Ppp1r1b, Oprm1, Grik3, and Cnr1. Distinct clusters demonstrate subtype-specific enrichment, indicating heterogeneity in MSN subtype specification after NeuroD1-induced reprogramming.

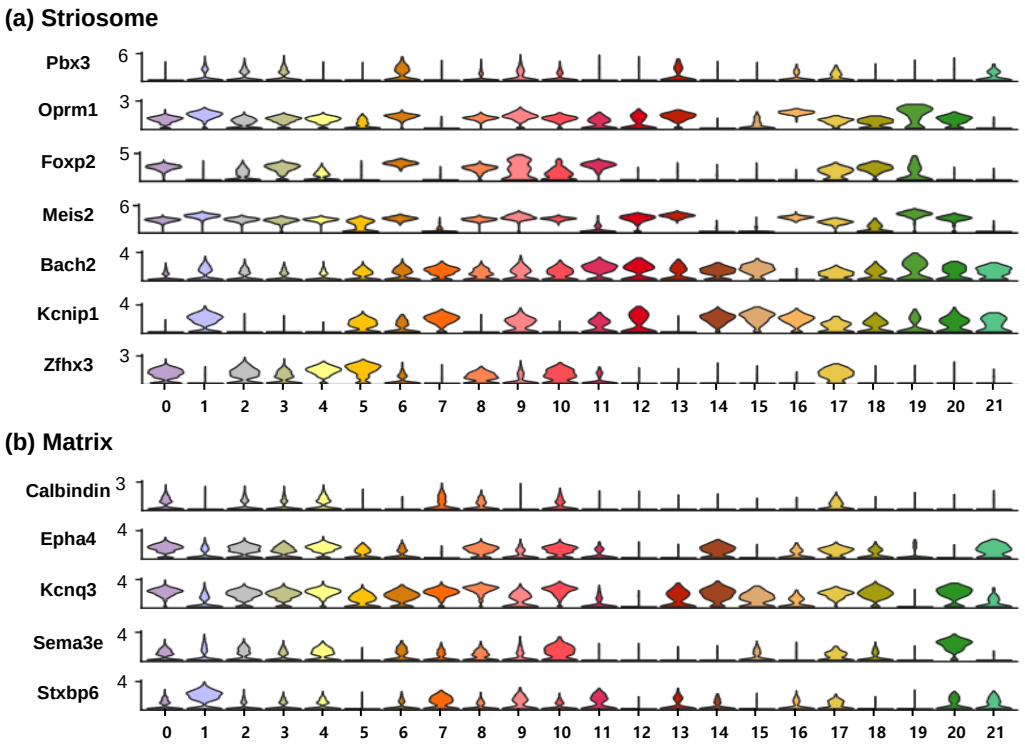

Figure 26. Violin plots of additional MSN subtype and compartment-specific markers across clusters

Expression levels of genes associated with striatal MSN subtypes and compartment identity across clusters 0–21 in NeuroD1-induced GABAergic populations. (a) Expression of Pbx3, Oprm1, Foxp2, Meis2, Bach2, Kcnip1, and Zfhx3, associated with striosome compartment identity. (b) Expression of Calbindin, Epha4, Kcnq3, Sema3e, and Stxbp6 is associated with matrix compartment identity. Cluster-specific expression patterns highlight the heterogeneity and compartmental specification of NeuroD1-converted striatal neurons.

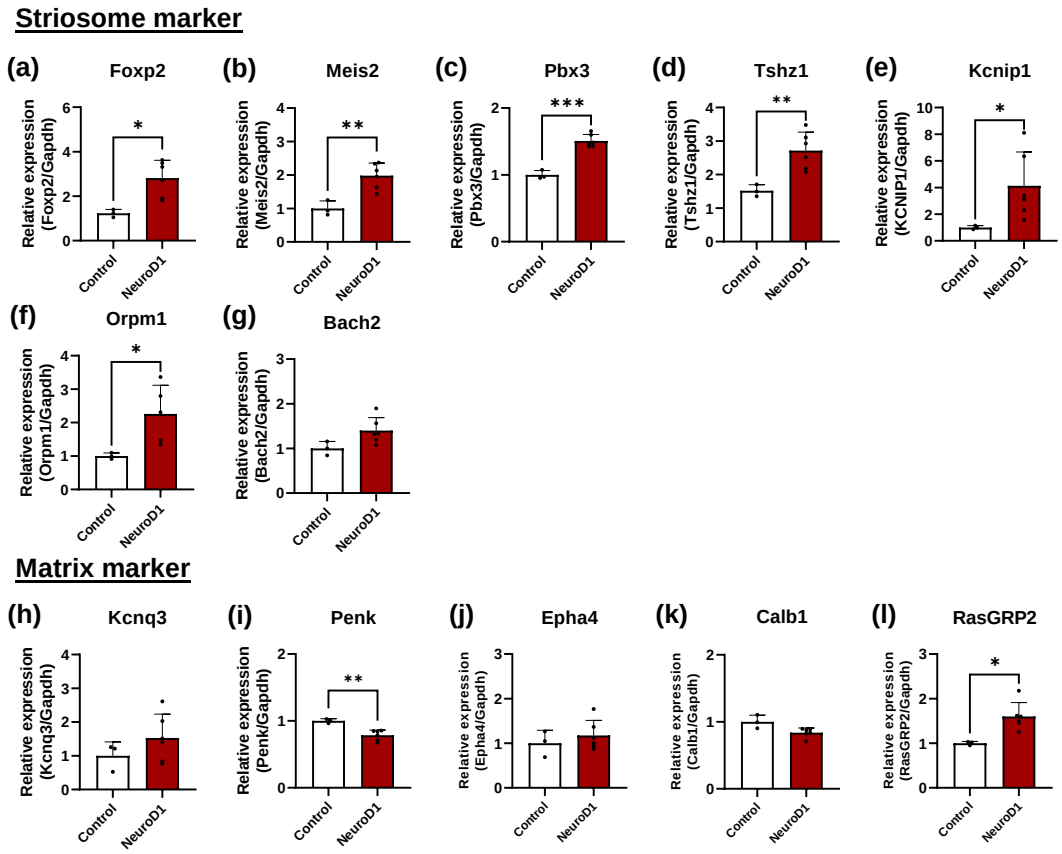

Figure 27. Validation of striosome and matrix marker expression in NeuroD1-treated striatal tissue

(a–g) Striosome markers: Foxp2, Meis2, Pbx3, Tac1, Kcnip1, Oprm1, and Bach2. (h–l) Matrix markers: Kcnq4, Penk, Epha4, Calb1, and RasGRP2. Striosome genes were significantly upregulated, whereas matrix markers demonstrated little or no change.

5. NeuroD1-Mediated GABAergic Reprogramming Restores Functional Maturity and Motor Behavior in HD

To identify whether NeuroD1-induced GABAergic neurons acquire functional maturity *in vivo*, the expression of chloride transporters KCC2 (Slc12a5) and NKCC1 (Slc12a2), which regulate inhibitory GABAergic signaling, was assessed. Western blot analysis revealed that KCC2 expression, which was significantly downregulated in HD striatum, was restored in the NeuroD1-treated group, whereas NKCC1 expression remained unchanged (Fig. 28a–c). These changes were corroborated by violin plots illustrating Slc12a5 upregulation in NeuroD1-enriched clusters in single-nucleus RNA sequencing (snRNA-seq) data (Fig. 28e), indicating improved chloride extrusion capacity and GABAergic neuron maturation.

To assess the functional consequences of these molecular changes, a battery of motor behavior tests was conducted in HD mice. NeuroD1-treated animals demonstrated significantly improved performance in the rotarod test, particularly at 8 and 12 wpi, indicating enhanced motor coordination (Fig. 29a–d). Further, grip strength and clasping scores, which reflect neuromuscular and dystonia-like symptoms, were significantly improved in the NeuroD1 group compared to HD controls (Fig. 29e–h). These results indicated that NeuroD1 not only induces GABAergic reprogramming but also contributes to behavioral recovery, potentially by restoring inhibitory circuit balance in the HD striatum.

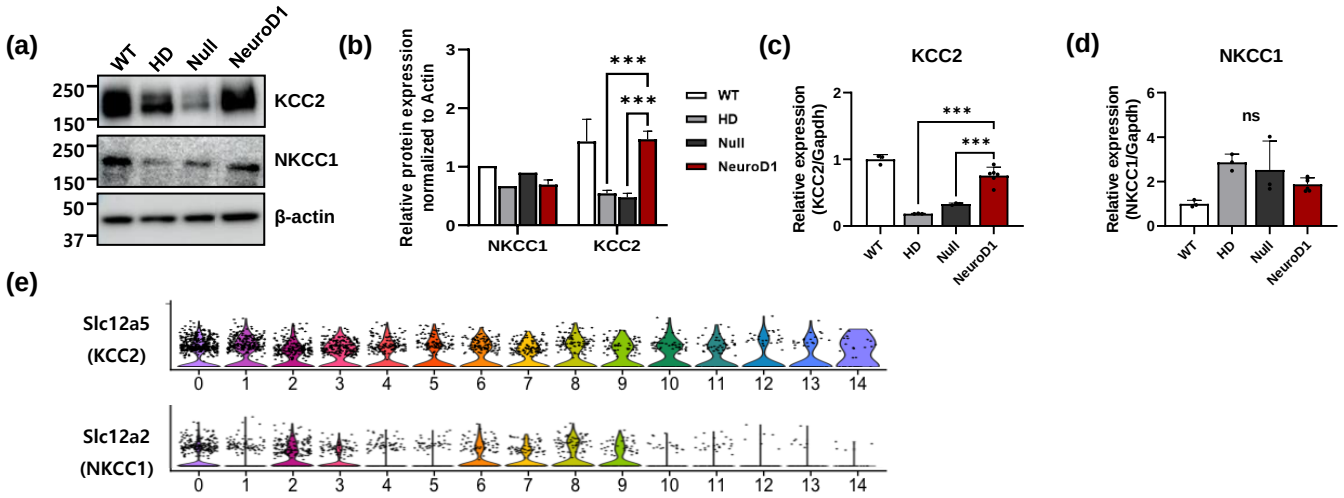

Figure 28. Restoration of chloride homeostasis via KCC2 upregulation in NeuroD1-treated HD mice

(a) Western blot analysis of KCC2 and NKCC1 expression in WT, HD, and NeuroD1-treated striatal. (b) Quantification of protein expression relative to β-actin. (c) Significant KCC2 upregulation in the NeuroD1 group. (e) Violin plots illustrating Slc12a5 (KCC2) upregulation and unchanged Slc12a2 (NKCC1) expression across snRNA-seq clusters.

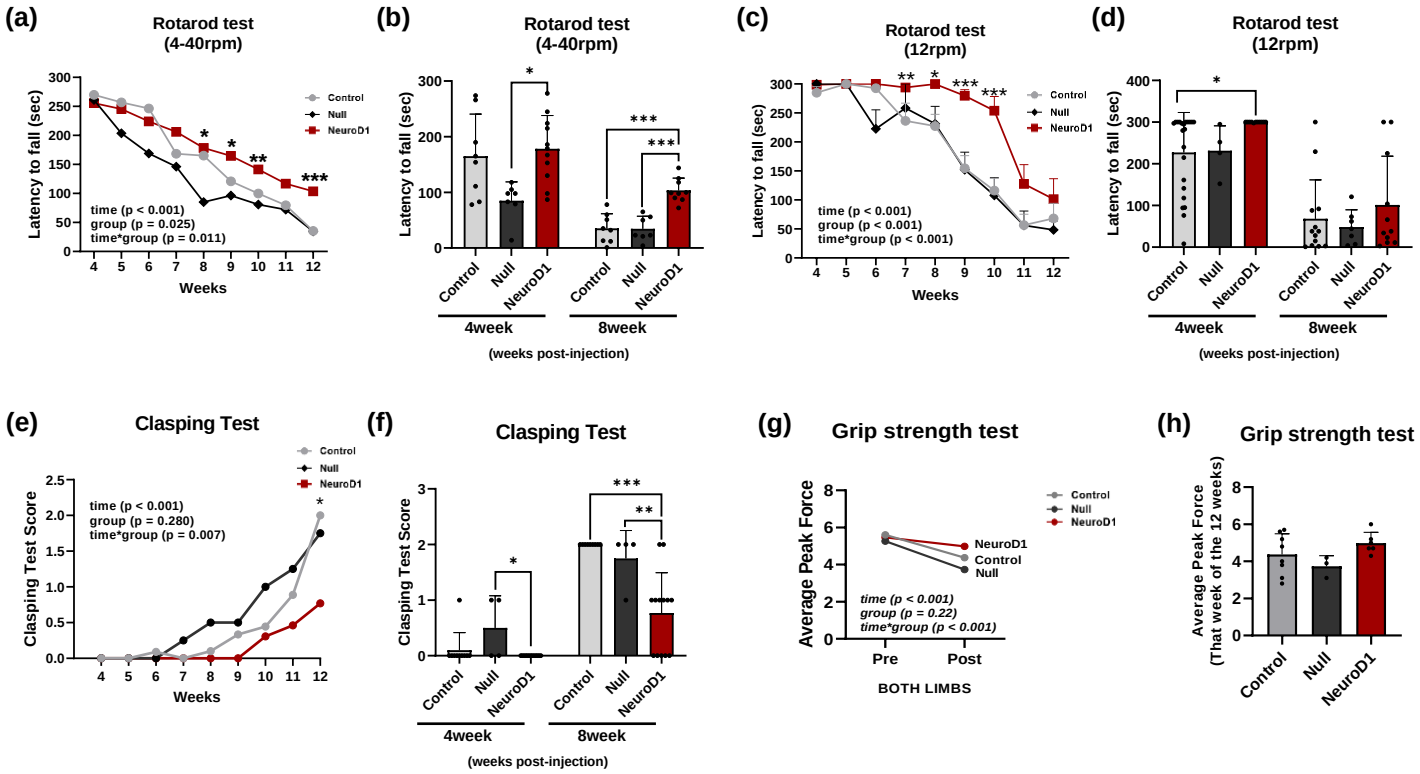

Figure 29. NeuroD1 treatment improves motor function and alleviates motor symptoms in HD mice

(a–b) Rotarod test (4–40 rpm) revealed significantly improved motor coordination in the NeuroD1-treated group, with prolonged latency to fall at both 4 and 8 wpi compared to the null group. (c–d) At a higher rotarod speed (12 rpm), the NeuroD1 group exhibited better motor performance over time compared to the null group, indicating improved balance and

endurance. (e–f) Clasping behavior, which is a marker of motor deterioration, was significantly suppressed in the NeuroD1-treated group, as demonstrated by lower clasping scores and reduced numbers of clasping-positive mice. (g–h) Grip strength was either preserved or slightly improved in the NeuroD1 group at 12 wpi, indicating maintenance of forelimb muscle function relative to the null mice.

Part3. Convergent Mechanisms Underlying Ascl1 and NeuroD1-Mediated Astrocytic Reprogramming and Striatal Repair in HD

1. Subtype-biased clustering of GABAergic neurons induced by Ascl1 or NeuroD1

To further analyze the impact of Ascl1 and NeuroD1 on GABAergic neuron subtype specification, more inclusive treatment-specific clustering of immature and mature neuronal populations was conducted using UMAP analysis, manually selecting GABAergic clusters for further analysis of striosome and matrix populations. This finding revealed distinct patterns of cluster expansion between the two groups (Fig. 32a–f). Ascl1-treated samples demonstrated enrichment in clusters 0, 4, 5, 6, 7, 8, 13, 14, 15, and 17, whereas NeuroD1-treated samples exhibited increased representation in clusters 1, 8, 9, 10, 12, 13, 16, 19, and 20. Cluster 13 was common to both groups.

The cellular identities of these clusters were then characterized using canonical markers of interneurons, neural progenitors, and MSNs (Fig. 33). Expression of Gad1, Gad2, and Pax2 indicated that clusters 11 and 19 (Ascl1 group) and clusters 7, 14, 15, and 21 (NeuroD1 group) were enriched in interneuron-like populations. Further, Dlx1 expression was broadly observed in multiple expanded clusters in both groups, indicating that many of the reprogrammed cells remained in an immature GABAergic state.

Together, these results demonstrated that both Ascl1 and NeuroD1 can induce GABAergic neurogenesis, but they give rise to heterogeneous populations, including interneurons and immature precursors. Marker-based analysis was conducted in subsequent sections to assess whether these reprogrammed cells acquire striosome or matrix MSN subtype identities.

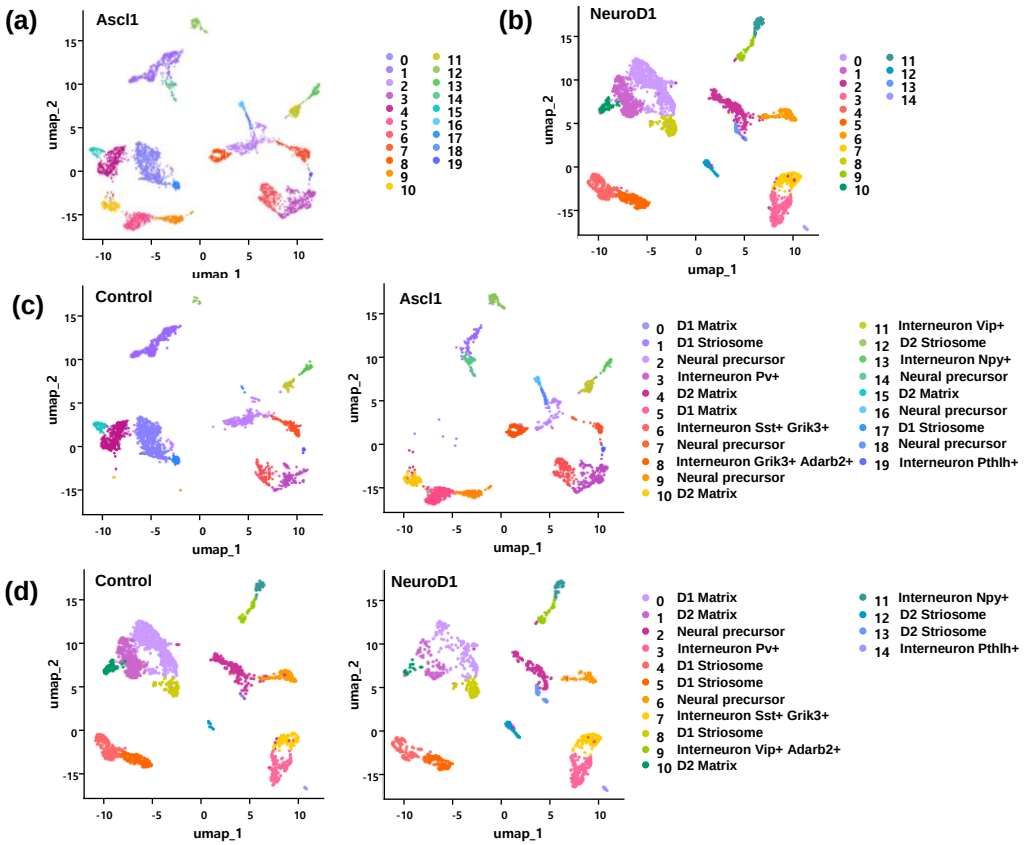

Figure 30. UMAP-based clustering of GABAergic cells across control, Ascl1, and NeuroD1 conditions

(a) UMAP plot illustrating clustering of GABAergic cells derived from all three conditions (control, Ascl1, and NeuroD1), jointly analyzed using Seurat. (b) Cells from the control and Ascl1 groups mapped onto the common UMAP space. Ascl1 cells were clustered into 20 groups (clusters 0–19). (c) Cells from the control and NeuroD1 groups mapped similarly. NeuroD1 cells were clustered into 15 groups (clusters 0–14). This integrated clustering enables direct comparison of condition-specific cluster occupancy and cell distribution. Cluster color coding is consistent across all panels.

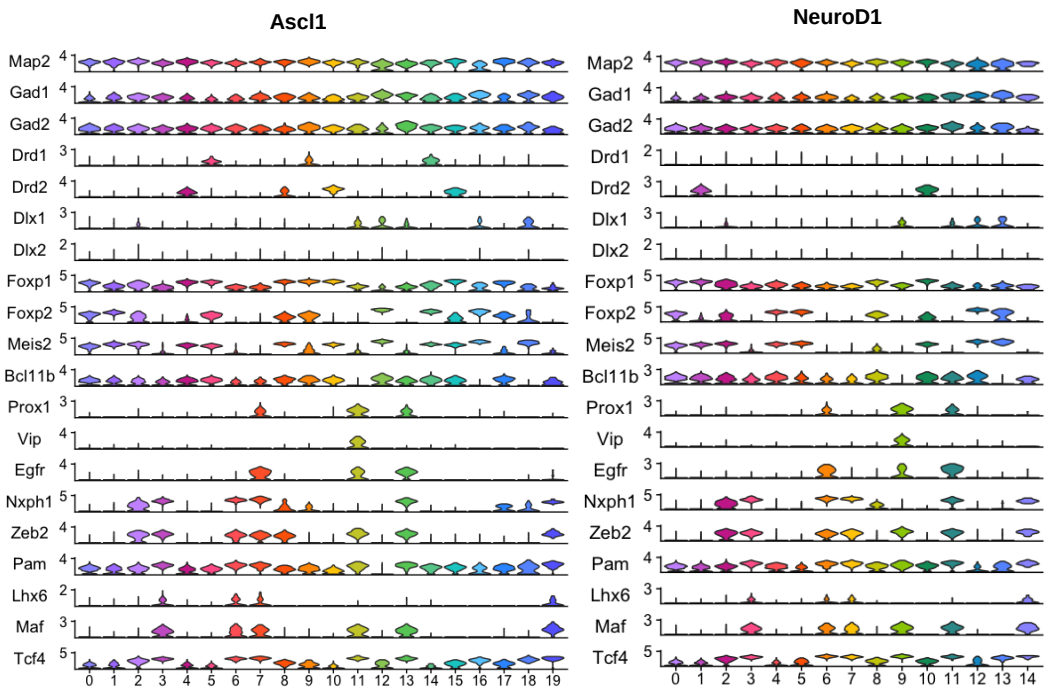

Figure 31. Expression of neuronal subtype markers in Ascl1- and NeuroD1-treated groups

Violin plots illustrating the expression of neuronal markers across clusters in the Ascl1 (left, clusters 0–19) and NeuroD1 (right, clusters 0–14) groups. Genes include pan-neuronal markers (*Map2*, *Gad1*, and *Gad2*), dopaminergic markers (*Drd1* and *Drd2*), transcription factors related to GABAergic identity (*Dlx1*, *Dlx2*, *Foxp1*, *Foxp2*, *Meis2*, and *Bcl11b*), and other subtype- or region-specific markers (*Prox1*, *Vip*, *Egfr*, *Nxph1*, *Zeb2*, *Pam*, *Lhx6*, *Maf*, and *Tcf4*). Cluster-specific expression patterns highlight the differences in the neuronal subtype compositions of Ascl1- and NeuroD1-induced GABAergic populations.

2. Reprogrammed Neurons Demonstrate Striosome-Biased D2-Type MSN Identity With Divergent Maturity

To further dissect the subtype and compartment identity of neurons reprogrammed by Ascl1 and NeuroD1, the expression patterns of D1/D2-type MSN subtype markers and striosome–matrix compartment markers across their respective clusters were analyzed (Fig. 32–34).

Violin plots illustrated that D1-type markers, including Drd1 and Foxp1, were selectively enriched in specific clusters in both groups (Fig. 32). Notably, Foxp1 expression exhibited a broader distribution in the NeuroD1 group, indicating enhanced D1 MSN specification. In contrast, D2-type markers—Drd2, Foxp2, Meis2, Pam, and Zeb2—were more strongly and widely expressed across the clusters in the NeuroD1-treated population, indicating robust differentiation toward the D2-type MSN fate compared to the Ascl1-treated population. Striosome–matrix compartment identity was further examined (Fig. 33). Striosome markers (Pbx3, Oprm1, Foxp2, and Meis2) were enriched in distinct clusters of both Ascl1 and NeuroD1 groups, supporting successful induction of striosomal characteristics. However, matrix markers (Epha4, Calb1, and Rasgrp2) demonstrated broader and more intense expression in the NeuroD1-treated group, indicating that NeuroD1 more effectively promotes matrix-like fate. Finally, cluster-specific mapping of these identities on UMAP plots was visualized (Fig. 34). NeuroD1-induced neurons demonstrated a balanced distribution of striosome-like (e.g., clusters 4, 5, 12, 13, 17) and matrix-like (e.g., clusters 0, 1, 4, 5, 10) populations, indicating parallel compartmental reconstitution. In contrast, Ascl1-treated neurons exhibited primary enrichment of striosome-like clusters (e.g., 12, 17) while failing to recover matrix-associated clusters that were otherwise present in the control group.

Taken together, these results indicated that NeuroD1 induces a broader spectrum of MSN subtypes and compartment identities, whereas Ascl1 induces a more striosome-restricted reprogramming pattern, thereby emphasizing transcription factor-specific outcomes in striatal neuronal fate specification.

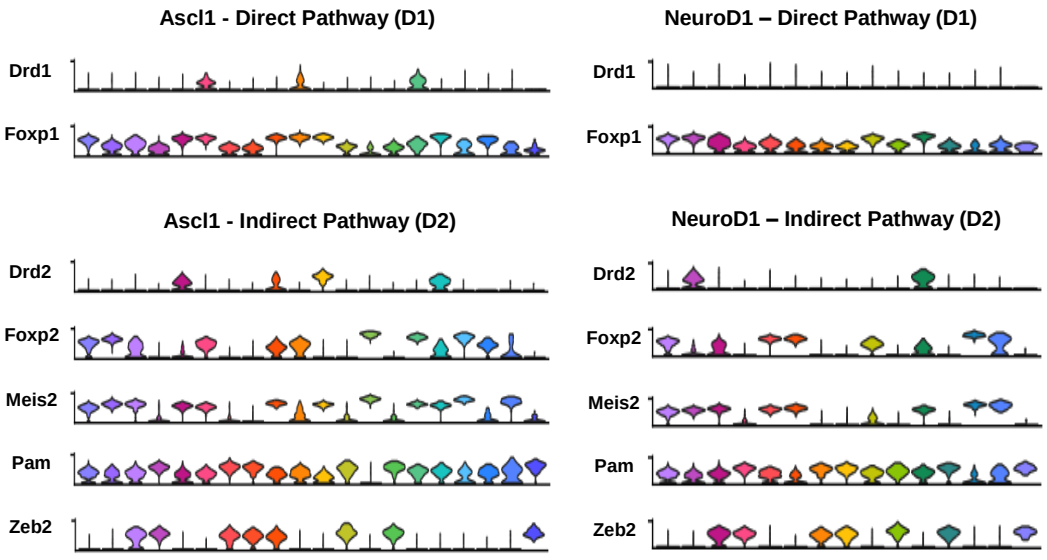

Figure 32. Expression of D1/D2-type MSN subtype markers in Ascl1- and NeuroD1-treated groups

Violin plots illustrate the cluster-specific expression of genes associated with D1- and D2-type MSNs in the Ascl1- (left, clusters 0–19) and NeuroD1-treated group (right, clusters 0–14). D1-type markers, including Drd1 and Foxp1, were selectively enriched in a subset of clusters in both groups, with Foxp1 demonstrating broader distribution in the NeuroD1 condition. D2-type markers, such as Drd2, Foxp2, Meis2, Pam, and Zeb2, were highly and more widely expressed in the NeuroD1-treated clusters compared to the Ascl1-treated clusters.

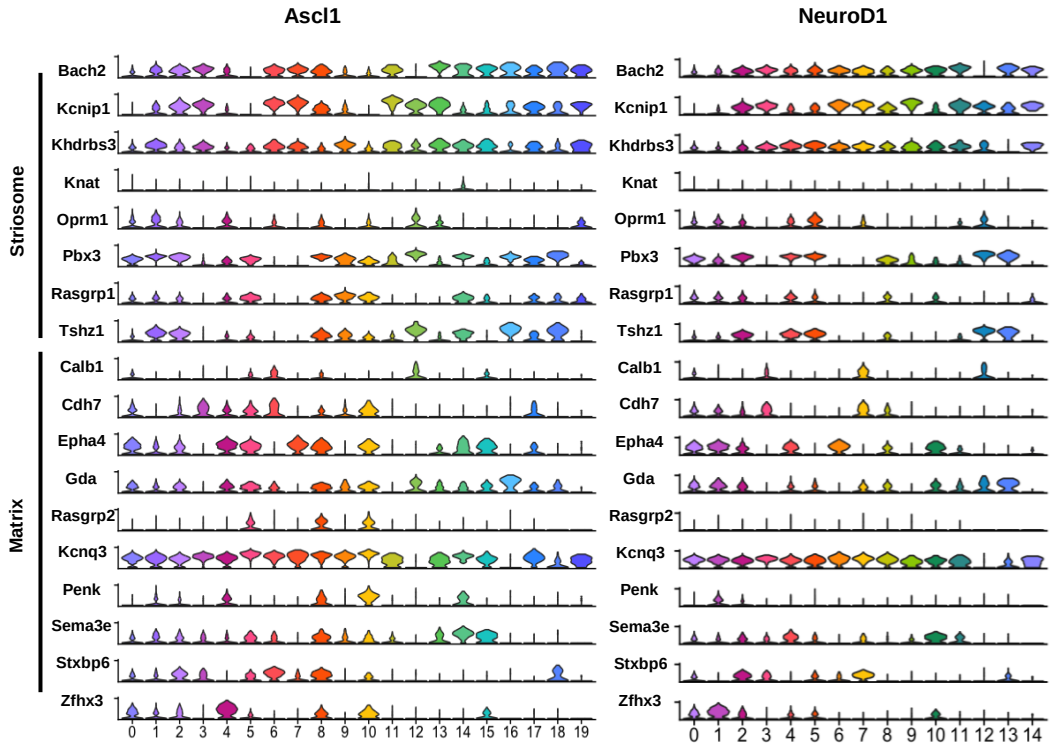

Figure 33. Cluster-specific expression of striosome- and matrix-associated genes in Ascl1- and NeuroD1-treated groups

Violin plots illustrate the expression of genes related to striosome and matrix compartment identity across clusters 0–19 (Ascl1, left) and 0–14 (NeuroD1, right). Striosome-related genes, such as *Pbx3*, *Oprm1*, *Foxp2*, and *Meis2*, were selectively enriched in distinct clusters of both groups, whereas matrix-associated markers, including Epha4, Calb1, and Rasgrp2, demonstrated broader and stronger expression, particularly in the NeuroD1 group. These differential expression patterns indicate that Ascl1 and NeuroD1 drive distinct compartmental specification during striatal neuronal reprogramming.

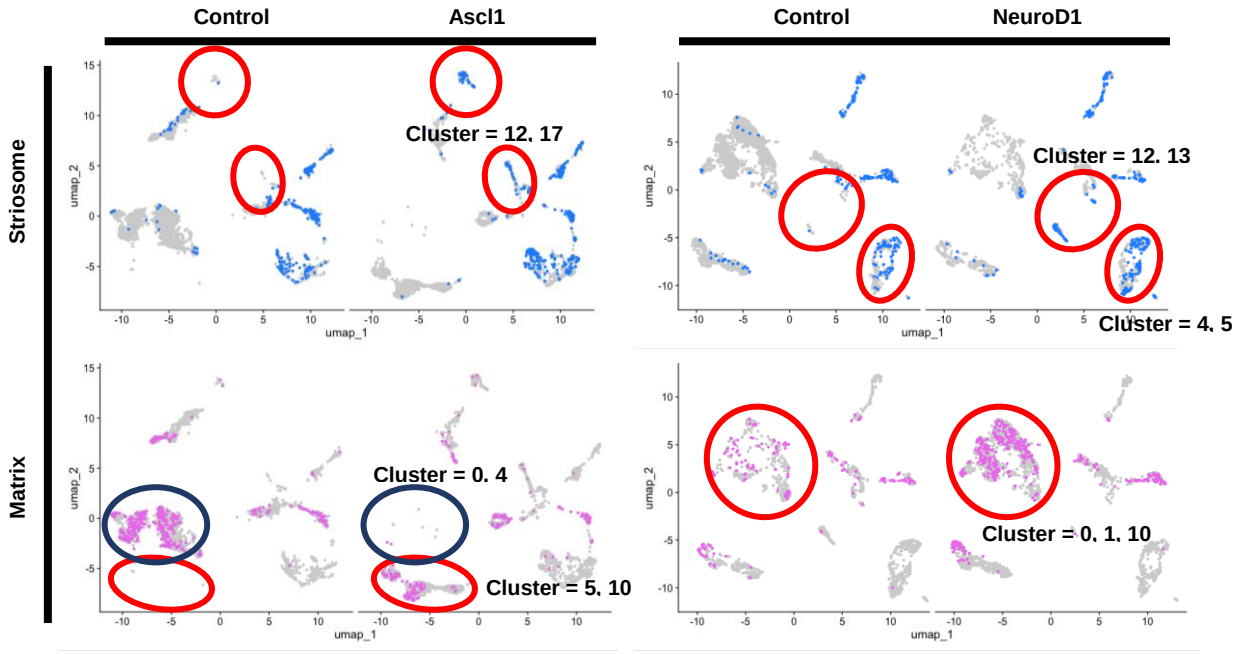

Figure 34. Cluster-specific mapping of striosome and matrix identities in NeuroD1- and Ascl1-treated neurons

UMAP plots illustrating clusters enriched for striosome (blue) and matrix (magenta) markers after NeuroD1 or Ascl1 treatment. NeuroD1 induced both striosome-like (clusters 4, 5, 12, 13, and 17) and matrix-like (clusters 0, 1, 4, 5, and 10) identities, marked by genes such as *Pbx3*, *Meis2*, *Oprm1*, *Calbindin*, and *Rasgrp2*. In contrast, Ascl1 induced enrichment of striosome clusters (12, 17) but a notable loss of matrix clusters that were present in the control group.

3. Astrocyte-to-neuron conversion induces time-dependent reduction of GFAP and increases in DARPP32$^+$ and GABA$^+$ neurons

To assess the efficacy of astrocyte-to-neuron conversion by Ascl1 or NeuroD1 *in vivo*, immunohistochemical quantification of astrocytic and neuronal markers in the striatum was performed at 4 and 8 wpi (Fig. 35). At 8 wpi, GFAP fluorescence intensity was significantly reduced in both Ascl1- and NeuroD1-treated groups compared to the control group, indicating effective astrocyte depletion. Notably, the NeuroD1 group demonstrated the most substantial reduction in GFAP expression, indicating more efficient astrocytic reprogramming (Fig. 35a). This pattern was consistent in the longitudinal comparison, with the NeuroD1 group demonstrating the steepest decline in GFAP intensity between 4 and 8 wpi (Fig. 35b).

Concomitantly, the number of DARPP32$^+$ MSNs was significantly increased in both treatment groups at 8 wpi, with the NeuroD1 group demonstrating a significantly higher density than the Ascl1 group, indicating improved MSN subtype reconstitution (Fig. 35c). Time-course analysis further validated a robust expansion of DARPP32$^+$ neurons in the NeuroD1-treated group compared to the others (Fig. 35d). Similarly, the number of GABA$^+$ neurons, indicative of GABAergic identity acquisition, was markedly increased in both Ascl1- and NeuroD1-treated groups at 8 wpi, with the NeuroD1 group exhibiting significantly higher levels than the Ascl1 group (Fig. 35e). The longitudinal trend mirrored this result, with the NeuroD1 group demonstrating the most pronounced increase in GABA$^+$ cell density over time (Fig. 35f).

Taken together, these results indicated that both Ascl1 and NeuroD1 successfully induced astrocyte-to-neuron conversion *in vivo*, but NeuroD1 exhibited a more robust and efficient transition, reflected by greater astrocyte depletion and stronger induction of DARPP32$^+$ and GABA$^+$ neuronal phenotypes.

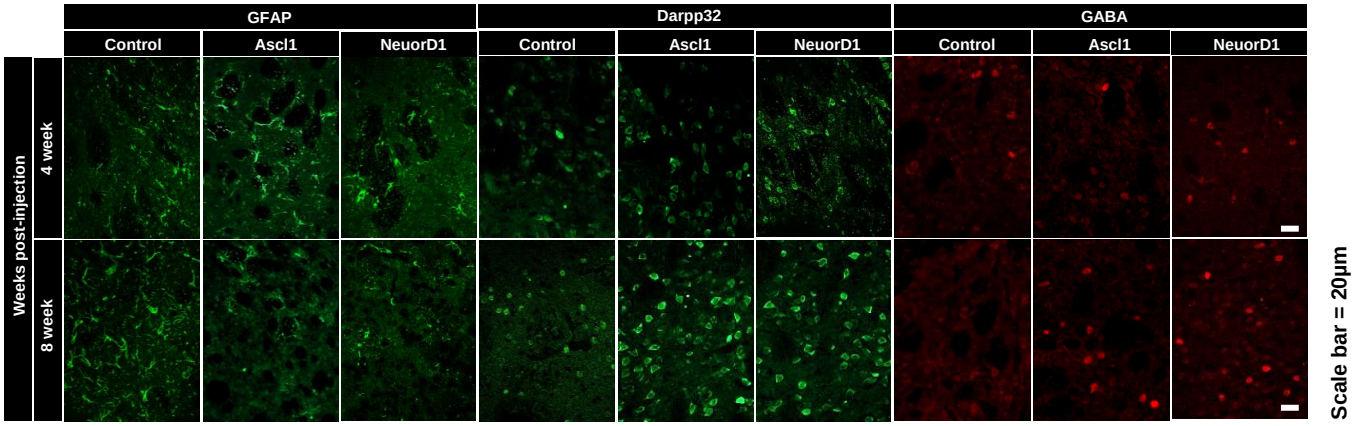

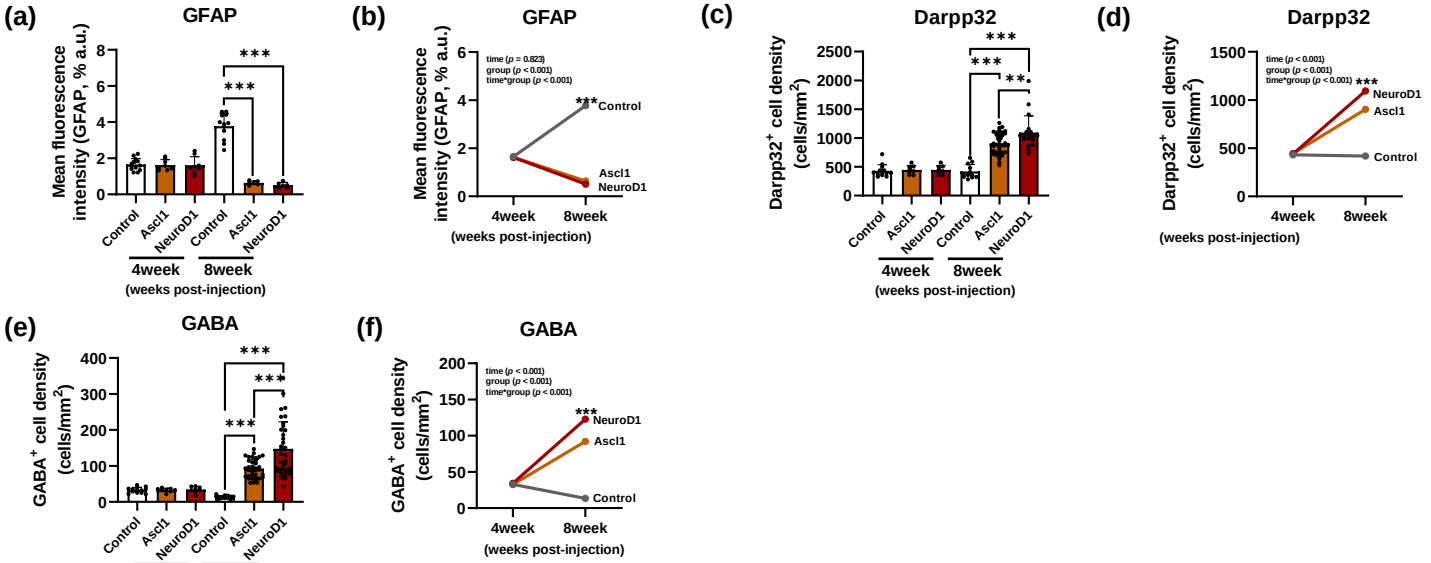

Figure 35. Quantitative analysis of GFAP, DARPP32, and GABA expression after Ascl1 or NeuroD1 treatment

(a) At 8 wpi, both Ascl1- and NeuroD1-treated groups demonstrated significantly reduced GFAP intensity compared to the control group ($p < 0.001$), with the NeuroD1 group exhibiting the most substantial reduction. (b) The line graph illustrates a marked time-dependent decrease, particularly in the NeuroD1 group. (c) $DARPP32^+$ neurons significantly increased in both Ascl1 ($p < 0.01$) and NeuroD1 ($p < 0.001$) groups at 8 wpi compared to the control group. Further, NeuroD1 demonstrated a higher cell density than Ascl1 ($p < 0.01$). (d) Time-dependent increase in $DARPP32^+$ cell number was most prominent in the NeuroD1-treated group. (e) The number of $GABA^+$ neurons significantly increased in both treatment groups at 8 wpi (Ascl1: $p < 0.01$ and NeuroD1: $p < 0.001$ vs. control), with the NeuroD1 group exhibiting a significantly higher number of $GABA^+$ neurons than the Ascl1 group ($p < 0.001$). (f) Time-course analysis reveals the most substantial increase in the NeuroD1-treated group. Data are presented as mean ± SEM. Statistical significance was assessed with one-way or two-way ANOVA followed by a Bonferroni post-hoc test.

4. Restoration of Striosomal Fate Via PBX3 and EPHA4 Expression

The striosome and matrix compartments represent structurally and transcriptionally distinct domains within the striatum. Disruption of the balance between these compartments is closely associated with emotional and behavioral impairments, particularly in neurodegenerative disorders such as HD. To identify whether astrocyte-to-neuron reprogramming with Ascl1 or NeuroD1 could restore striosomal identity, the expression of PBX3 and EPHA4—key markers involved in striatal compartmentalization—was assessed.

PBX3 is a well-established marker of the striosomal compartment and was found in discrete patch-like regions in control animals. $PBX3^+$ cells were detected by immunostaining in both Ascl1- and NeuroD1-treated groups; however, the $PBX3^+$ area was significantly larger in the NeuroD1 group (Fig. 36a–c), indicating a more robust induction of striosome-specific fate. To further assess compartmental organization, EPHA4 was examined, which is a guidance molecule known to be preferentially expressed in the matrix compartment and crucial for establishing striosome–matrix boundaries. While not restricted to the striosome, EPHA4 expression provides structural cues for compartmental layout. Co-localization analysis in the NeuroD1 group revealed that $PBX3^+$ striosomal regions were often adjacent to or bordered by $EPHA4^+$ matrix regions (Fig. 36d–f), indicating improved spatial patterning and boundary definition between striosome and matrix compartments.

To validate these observations at the transcriptomic level, RT-qPCR analysis of striosome and matrix marker genes was conducted (Fig. 37). Striosomal markers (Foxp2, Meis2, Pbx3, Tshz1, and Oprm1) were significantly upregulated in the NeuroD1 group compared to both control and Ascl1 groups, indicating the re-establishment of striosomal identity at the molecular level. Meanwhile, the expression of matrix-related markers (Calb1, Epha4, and Rasgrp2) was moderately preserved, indicating that NeuroD1 promotes broad MSN subtype restoration.

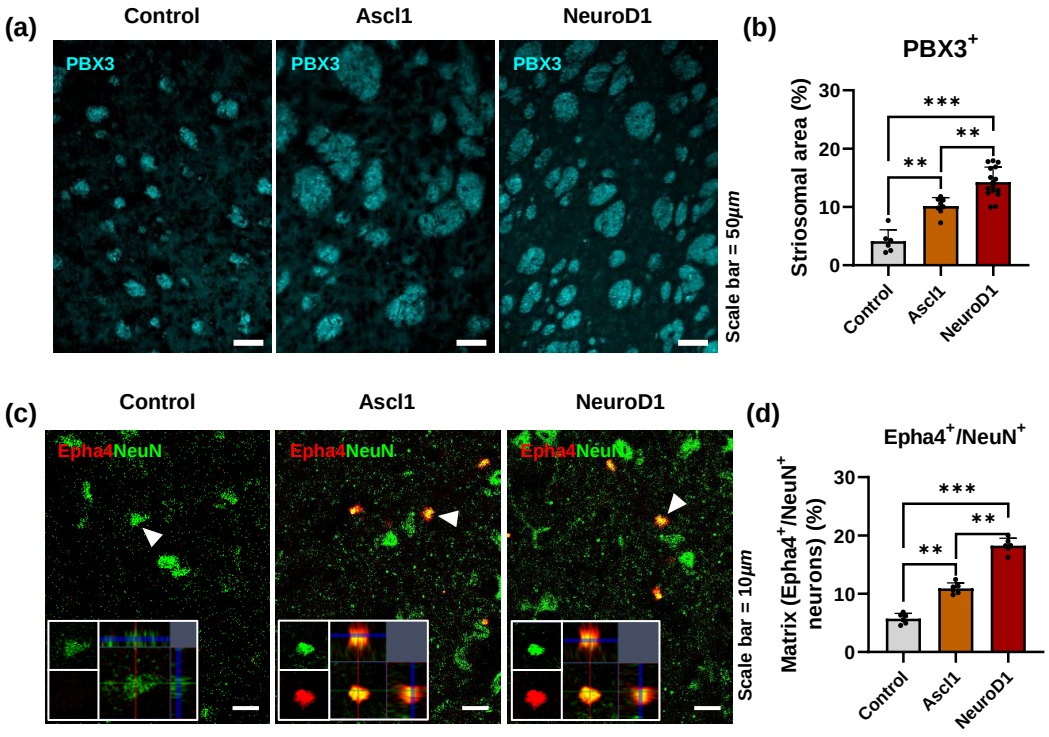

Figure 36. Immunostaining of PBX3 and Epha4 reveals the restoration of striosomal identity after Ascl1 and NeuroD1 treatment

(a) Representative immunofluorescence images demonstrating PBX3$^+$ cells in the striatum of control, Ascl1, and NeuroD1 groups. PBX3, which is a striosome-specific marker, demonstrated compartmental distribution that indicates striosomal domains. Scale bar = 50 μm. (b) PBX3$^+$ striosomal area quantification (% of total striatal area). Both Ascl1 and NeuroD1 treatments significantly increased the PBX3$^+$ area, with NeuroD1 exhibiting a stronger effect. (c) Representative images of Epha4 (red) and NeuN (green) double immunostaining in the striatum. Arrowheads denote Epha4$^+$/NeuN$^+$ neurons. Insets show high-magnification views, with orthogonal projections confirming co-localization. Scale bar = 10 μm. (d) Quantification of Epah4$^+$/NeuN$^+$ double-positive neurons in matrix regions. Both Ascl1 and NeuroD1 increased the proportion of Epha4$^+$ neurons among

NeuN^{+} cells, with the NeuroD1 group exhibiting the most significant increase. These results demonstrated that both Ascl1 and NeuroD1 effectively promote striosomal fate acquisition in the striatum, with NeuroD1 exhibiting a more robust effect, as indicated by the greater expansion of PBX3^{+} regions and EPHA4^{++}neuronal populations.

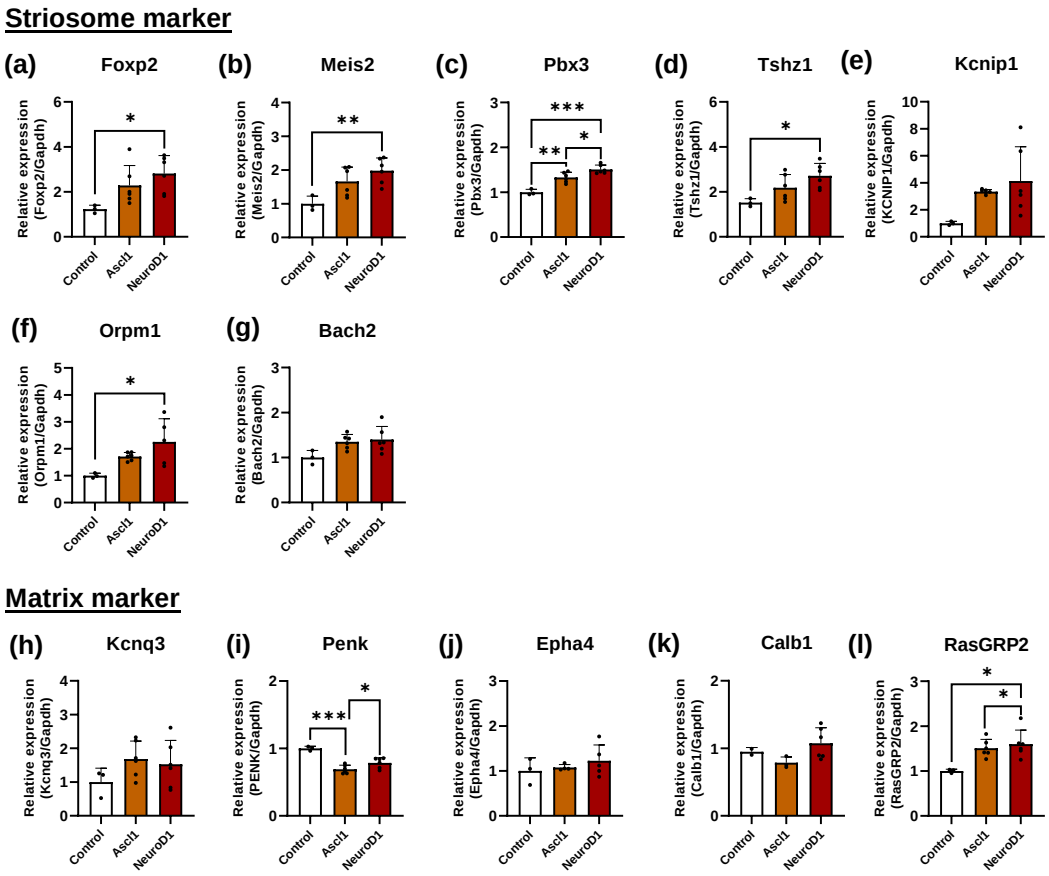

Figure 37. qPCR validation of striosome and matrix marker gene expression

Bar graphs illustrating mRNA expression of striosomal markers (*Foxp2*, *Meis2*, *Pbx3*, *Tshz1*, and *Oprm1*) and matrix markers (*Calb1*, *Rasgrp2*, and *Epha4*) across control, Ascl1, and NeuroD1 groups. NeuroD1 significantly upregulated striosomal genes and partially preserved matrix-related gene expression.

5. NeuroD1-Mediated Neuronal Reprogramming Improves Motor and Reflex Function in HD Mice

To assess the functional outcomes of astrocyte-to-neuron conversion *in vivo*, a battery of behavioral tests was conducted using the R6/2 HD mouse model. Mice received striatal Ascl1 or NeuroD1 injections and were assessed longitudinally for motor coordination, muscle strength, and reflex abnormalities.

The rotarod test, which measures motor balance and endurance, revealed that NeuroD1-treated mice demonstrated significantly better performance across all time points compared to both control and Ascl1-treated groups (Fig. 38a–c). The latency to fall was markedly prolonged in the NeuroD1 group, especially under accelerating speed conditions (4–40 rpm). At 12 wpi, rotarod performance declined in all groups, but the NeuroD1 group still retained superior performance compared to others (Fig. 38d).

Muscle strength was assessed using a grip strength test. All groups exhibited a general decline over time, whereas NeuroD1-treated mice maintained slightly better forelimb and hindlimb strength than Ascl1-treated or control mice (Fig. 38e–f). To assess reflex integrity and neurodegeneration, the clasping test, which is a standard measure of dystonia-like symptoms in HD models, was performed. NeuroD1-treated mice exhibited a significant delay in clasping onset and lower clasping scores over time, indicating reduced reflex impairment and delayed disease progression (Fig. 38g–h).

Taken together, these results revealed that NeuroD1 reprogramming results in more substantial motor and behavioral recovery in HD mice compared with Ascl1, probably due to the induction of more mature and subtype-diverse MSNs, including both striosomal and matrix populations.

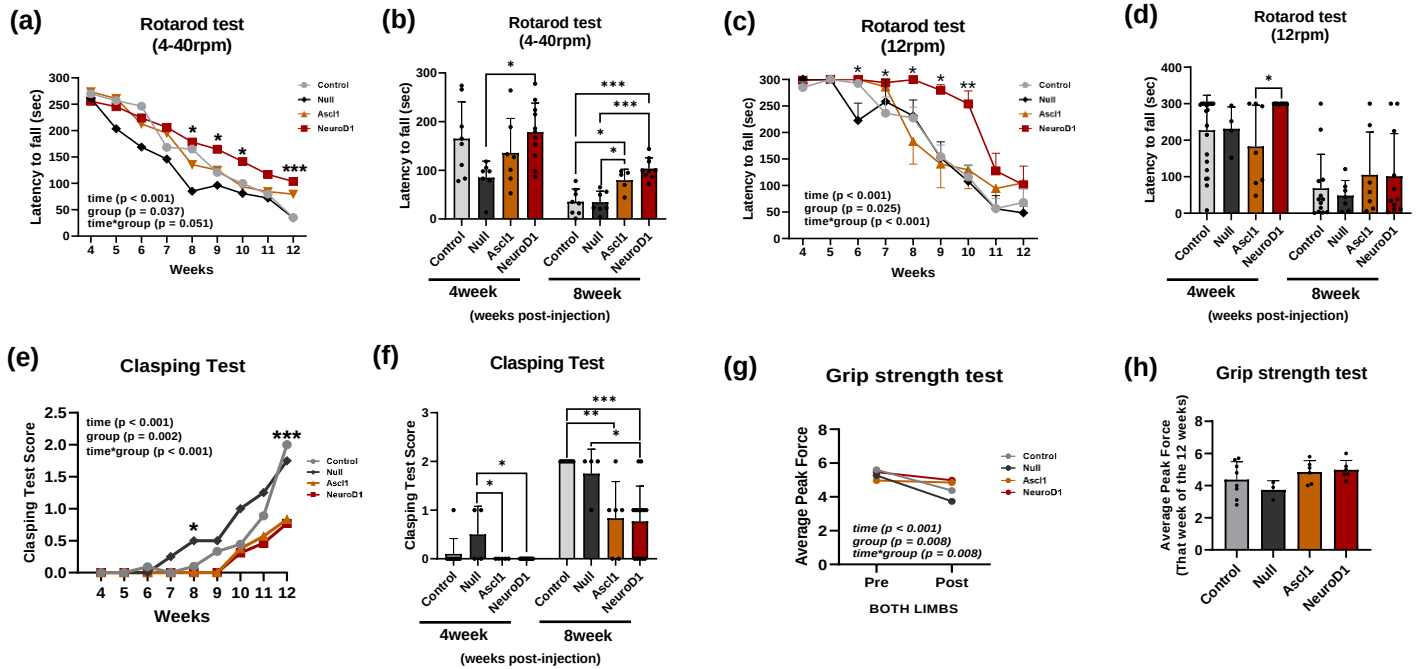

Figure 38. Both Ascl1 and NeuroD1 improve motor behavior in HD mice, with NeuroD1 demonstrating superior and more sustained effects

(a, b) Rotarod performance at 4 rpm demonstrated increased latency to fall in the Ascl1- and NeuroD1-treated groups compared to the null group. Among them, NeuroD1 consistently induced the greatest improvement in motor coordination. (c, d) At 12 rpm, both treatment groups outperformed the null group, but NeuroD1-treated mice maintained higher latency times and greater stability throughout the testing period. (e, f) Clasping behavior worsened over time in the null group,

whereas both Ascl1 and NeuroD1 significantly reduced clasping scores and the percentage of clasping-positive animals. NeuroD1 exhibited a stronger suppressive effect on pathological behavior. (g, h) Grip strength was best preserved in the NeuroD1 group, as indicated by higher peak force values compared to the null and Ascl1 groups.

4.DISCUSSION

The present study investigated whether the direct reprogramming of astrocytes into GABAergic neurons with Ascl1 or NeuroD1 could restore the striatal MSN identity, particularly focusing on striosome and matrix subtype specification and functional recovery in an HD model[18, 19, 21]. Our results demonstrated that both transcription factors successfully induced GABAergic neuron formation, yet they exhibited marked differences in the resulting neuronal subtypes, maturation states, and behavioral outcomes. These findings contribute to the growing body of literature emphasizing the role of lineage-specific transcription factors in guiding neuronal identity and compartmental fate, particularly in disease contexts where specific subpopulations, such as striosomal D2-type-MSN, are selectively vulnerable[1, 3].

GABAergic Induction and MSN Subtype Specification

UMAP-based clustering and marker analysis of snRNA-seq data revealed that both Ascl1 and NeuroD1 robustly induced GABAergic neuronal populations in the striatum of R6/2 mice[19, 24, 31]. Notable differences emerged in subtype identity and maturation level despite substantial overlap in the reprogrammed clusters between the two treatment groups. Ascl1 treatment predominantly led to immature GABAergic neurons, with strong expression of progenitor markers, such as *Dlx1* and *Epha5*[20, 26], with the latter specifically enriched in immature striosomes (Kelly et al., 2021), whereas NeuroD1 treatment formed more mature neuronal clusters with increased expression of Synpr, Htr7, and other markers, indicating D2-type MSNs[20, 31]. Interestingly, both factors converged on the generation of a large D2-type striosomal cluster, suggesting a shared ability to bias reprogramming toward this vulnerable population. However, the lower maturity and weaker matrix representation in the Ascl1 group indicate a limited reconstitution of the full MSN subtype spectrum.

Divergent Striosome/Matrix Fate and Neuronal Maturation

Subtype identity was further identified through module scoring using canonical markers for striosome (Meis2, Foxp2, Tshz1, and Oprm1) and matrix (Calb1, Rasgrp2, and Epha4) compartments[1, 6, 8]. These analyses revealed that NeuroD1-treated neurons demonstrated a broader diversity of striatal fates, including the retention of matrix-type MSNs, whereas Ascl1-induced neurons were largely restricted to the striosomal lineage[31, 33]. The high Meis2 expression in both groups supports a shared capacity to generate striosome-fated neurons[3, 6]. However, the broader repertoire of neuronal subtypes and decreased progenitor marker expression in NeuroD1-treated clusters emphasize its superior reprogramming efficiency[22, 24, 31]. The ability of NeuroD1 to generate more mature, subtype-diverse MSN populations may be related to its chromatin remodeling capabilities and epigenetic accessibility, consistent with previous studies identifying NeuroD1 as a potent driver of direct neuronal conversion.

Functional Outcomes and Behavioral Recovery

Importantly, behavioral analyses revealed the functional consequences of these transcription factor-induced differences[19, 31, 32]. NeuroD1-treated mice demonstrated significantly improved performance in terms of motor coordination and open field tests compared to Ascl1-treated mice[32, 33]. These improvements may stem from the dual effect of NeuroD1: the induction of more mature D2 striosomal MSNs, which are crucial for regulating reward and decision-making circuits, and the partial restoration of matrix-type MSNs, which integrate corticostriatal inputs required for motor execution[1, 8, 31]. The restoration of striosomal neurons has been emphasized due to their vulnerability and crucial roles in early HD pathogenesis; however, our findings indicated that matrix-type MSN preservation also significantly contributes to functional recovery. The combinatorial recovery of both compartments may underlie the more physiologically balanced restoration of striatal circuitry observed in the NeuroD1 group.

Interestingly, behavioral improvements were already evident at 8 wpi (4 weeks after viral delivery), particularly in the NeuroD1-treated group; however, corresponding molecular and histological analyses revealed no significant changes at this time point[31, 32]. Neither immunohistochemical staining nor qRT-PCR assessments of neuronal and glial markers revealed robust differences between treatment groups at 8 wpi, indicating a temporal lag between functional recovery and detectable cellular remodeling. This discrepancy implied that early behavioral gains might indicate circuit-level modulation or synaptic reorganization, potentially caused by NeuroD1's fast-acting effects on neuronal excitability and neurotransmitter balance[21, 24] rather than fully mature neuronal conversion.

Considering that transcription factor-induced reprogramming is a progressive process, newly generated neurons need to be initiated to integrate functionally into existing circuits before reaching full molecular or morphological maturity. In particular, partial functional identity acquisition—such as GABAergic activity or limited synaptic connectivity—may be sufficient to modulate motor outputs and reduce pathological behaviors in the early phase. At 12 wpi (8 weeks after viral treatment), these cellular changes became more clearly detectable at the gene and protein expression levels, more closely aligning with the observed behavioral phenotypes. Thus, the delayed convergence of molecular and functional readouts highlights the dynamic and staged nature of *in vivo* reprogramming and highlights the need to consider both early physiological modulation and later structural maturation when assessing therapeutic efficacy[21, 24, 33].

5. CONCLUSION

This study revealed the therapeutic potential of astrocyte-to-neuron conversion for restoring striatal circuits in the R6/2 mouse model of HD. Both Ascl1 and NeuroD1 successfully converted astrocytes into GABAergic neurons, but demonstrated distinct mechanisms and outcomes. Ascl1 primarily induced immature D2-type striosomal MSNs through an indirect, progenitor-like route, whereas NeuroD1 caused a more direct conversion into a diverse population of MSNs, encompassing both striosome and matrix subtypes.

Notably, NeuroD1 treatment led to the generation of more mature neurons and earlier and more sustained behavioral improvements, indicating successful integration of converted neurons into existing circuits. Behavioral recovery preceded detectable molecular and histological changes, indicating the dynamic and stepwise nature of *in vivo* astrocyte-to-neuron conversion, where early physiological modulation can occur before full structural maturation. Further, our results illustrated the importance of striatal striosomes as key players in not only limbic-feedback circuits but potentially as modulators of neurobehavioral and locomotor function. These findings provide strong evidence that subtype-specific astrocyte-to-neuron conversion contributes to compartment-targeted circuit repair and establishes a conceptual foundation for precision cell therapy in neurodegenerative disorders characterized by selective neuronal loss, such as HD.

REFERENCES

1. Arlotta P, et al. Transcriptional vulnerabilities of striatal neurons in human and rodent models of Huntington′s disease. Cell 2023.

2. Friedman A, et al. Striosomes control dopamine via dual pathways paralleling canonical basal ganglia circuits. Cell 2015;163(3):636–650.

3. Amemori K, et al. Striosomes and Matrisomes: Scaffolds for Dynamic Coupling of Volition and Action. Neuron 2023;111(9):1415–1430.

4. Graybiel AM, Matsushima A. Striosomes and Matrisomes: Scaffolds for Dynamic Coupling of Volition and Action. Annu Rev Neurosci 2023.

5. Brimblecombe KR, Cragg SJ. The Striosome and Matrix Compartments of the Striatum. ACS Chem Neurosci 2016;7(4):471–472.

6. Crittenden JR, Graybiel AM. Basal ganglia disorders associated with imbalances in the striatal striosome and matrix compartments. Front Neuroanat 2011;5:59.

7. Gerfen CR. The neostriatal mosaic: multiple levels of compartmental organization. Trends Neurosci 1992;15(4):133–139.

8. Fujiyama F, et al. Distinct connectivity of striosome and matrix compartments in the striatum. J Neurosci 2011;31(3):1035–1043.

9. Smith JB, Alloway KD. Functional specificity of corticostriatal projections in the rat. J Neurosci 2010;30(2):639–649.

10. Graybiel AM. Neurotransmitters and neuromodulators in the basal ganglia. Trends Neurosci 1990;13(7):244–254.

11. Calabresi P, et al. Direct and indirect pathways of basal ganglia: a critical reappraisal. Nat Neurosci 2014;17(6):766–773.

12. Gerfen CR, Surmeier DJ. Modulation of striatal projection systems by dopamine. Annu Rev Neurosci 2011;34:441–466.

13. Cazorla M, et al. Dopamine D2 receptors regulate the anatomical and functional balance of basal ganglia circuitry. Neuron 2014;81(1):153–164.

14. Lobo MK, et al. Cell type–specific loss of BDNF signaling mimics optogenetic control of cocaine reward. Science 2010;330(6002):385–390.

15. Durieux PF, et al. D2R striatopallidal neurons inhibit both locomotor and rewarding effects of cocaine. Nat Neurosci 2009;12(4):393–395.

16. Kravitz AV, et al. Regulation of parkinsonian motor behaviors by optogenetic control of basal ganglia circuitry. Nature 2010;466(7306):622–626.

17. Albin RL, et al. The functional anatomy of basal ganglia disorders. Trends Neurosci 1989;12(10):366–375.

18. Guo Z, et al. In vivo direct reprogramming of reactive glial cells into functional neurons after brain injury and in an Alzheimer′s disease model. Cell Stem Cell 2014;14(2):188–202.

19. Cheng L, et al. Direct conversion of astrocytes into neuronal cells by NeuroD1 induces neuroprotection in stroke. Cell Stem Cell 2014;14(2):179–187.

20. Liu Y, et al. Ascl1 converts dorsal midbrain astrocytes into functional neurons in vivo. J Neurosci 2015;35(25):9336–9355.

21. Niu W, et al. In vivo reprogramming of astrocytes to neuroblasts in the adult brain. Nat Cell Biol 2013;15(10):1164–1175.

22. Heinrich C, et al. Directing astroglia from the cerebral cortex into subtype specific functional neurons. PLoS Biol 2010;8(5):e1000373.

23. Torper O, et al. Generation of induced neurons via direct conversion in vivo. Proc Natl Acad Sci U S A 2015;112(17):11870–11875.

24. Matsuda T, et al. Pioneer factor Pax6 enables direct conversion of astrocytes into specific neuronal subtypes. Nat Commun 2019;10(1):3274.

25. Zhou H, et al. Conversion of reactive astrocytes to induced neurons enhances functional recovery after spinal cord injury. Nat Commun 2020;11(1):798.

26. Grande A, et al. Environmental impact on direct neuronal reprogramming in vivo in the adult brain. Nat Commun 2013;4(1):2373.

27. Berninger B, et al. Functional properties of neurons derived from in vivo reprogrammed astroglia. J Neurosci 2007;27(32):8654–8664.

28. Bateup HS, et al. Distinct subclasses of medium spiny neurons differentially regulate striatal

motor behaviors. Proc Natl Acad Sci U S A 2010;107(33):14845−14850.

29. Yin, H. H., & Knowlton, B. J. 2006. The role of the basal ganglia in habit formation. Nature Reviews Neuroscience, 76, 464−476.

30. Mallet, N., et al. (2012). Dichotomous organization of the external globus pallidus. Neuron, 746, 1075−1086.

31. Jiang, Y., et al. (2020). Direct neuronal reprogramming in vivo facilitates recovery of cognitive function after traumatic brain injury. Cell Reports, 308, 2499−2511.e6.

32. Wu, Z., et al. (2020). Gene therapy conversion of striatal astrocytes into GABAergic neurons in mouse models of Huntington′s disease. Nature Communications, 111, 1105.

33. Zhou, Y., et al. (2022). Glia-to-neuron conversion by CRISPR-CasRx alleviates symptoms of neurological disease in mice. Cell, 1853, 416−432.e21.

34. Qian, H., et al. (2020). Reversing a model of Parkinson′s disease with in situ converted nigral neurons. Nature, 5827813, 550−556.

35. Su, Z., et al. (2014). In vivo conversion of astrocytes to neurons in the injured adult spinal cord. Nature Communications, 5, 3338.

36. Gascón, S., et al. (2016). Identification and successful negotiation of a metabolic checkpoint in direct neuronal reprogramming. Cell Stem Cell, 183, 396−409.

37. Liu, Y., et al. (2020). Restoration of excitatory synaptic transmission in a Huntington′s disease model using direct glia-to-neuron conversion. Science Advances, 649, eabc7371.

38. Wang, L. L., et al. 2020. Reprogramming reactive glia into interneurons in the injured spinal cord with NeuroD1. Neuron, 1072, 306−321.e9.

39. Chang, Y. C., et al. 2021. A therapeutic strategy for spinal cord injury by converting reactive astrocytes into neurons. Cell Discovery, 71, 48.

40. Lee, K., et al. (2020). Modulation of direct glia-to-neuron conversion in Alzheimer′s disease model. Molecular Psychiatry, 2511, 2605−2618.

41. Tai, Y., et al. (2021). Enhancing astrocyte-to-neuron conversion using transcription factors and epigenetic modulators. Science Translational Medicine, 13593, eaba4414.

42. Matsuda, T., & Nakashima, K. (2021). Conversion of astrocytes to neurons using NeuroD1 improves synaptic function in mouse models of neurodegeneration. Stem Cell Reports, 164, 823–835.

43. Xue, Y., et al. (2021). Sequential transcription factor induction converts astrocytes to functional neurons in Alzheimer′s models. Nature Neuroscience, 244, 579–591.

44. Barker, R. A., & Götz, M. 2018. Treating neurodegenerative disease by reprogramming. Nature Reviews Neurology, 1410, 570–579.

45. He, Z., et al. (2017). Enhancing astrocyte-to-neuron reprogramming using small molecules. Cell Reports, 2112, 3416–3425.

46. Huang, Y., et al. (2020). Neural circuit repair through astrocyte-to-neuron conversion. Neuron, 1081, 99–114.e7.

47. Gao, L., et al. (2021). Glial reprogramming for neural repair: molecular mechanisms and therapeutic potential. Nature Reviews Neuroscienc, 228, 481–498.

48. Chen, W., et al. (2021). Direct in vivo reprogramming of reactive glia into GABAergic neurons after cerebral ischemia. Frontiers in Cell and Developmental Biology, 9, 682837.

49. Lu, Y., et al. (2022). Lineage reprogramming of astroglia into glutamatergic and GABAergic neurons in Huntington′s disease models. Nature Neuroscience, 259, 1227–1240.

50. Wang, C., et al. (2023). Functional integration of astrocyte-derived neurons into basal ganglia circuits. Science Advances, 912, eadh1468.

51. Cheng, L., et al. (2023). Regeneration of the basal ganglia by direct reprogramming of astrocytes into neurons. Nature Cell Biology, 252, 185–198.

52. Zhou, T., et al. (2023). Astrocyte-derived neurons exhibit subtype-specific integration in striatal circuits. Nature Neuroscience, 263, 402–416.

53. Sathyamurthy, A., et al. (2022). Direct reprogramming reveals subtypes of striatal neurons. Cell Reports, 389, 110391.

54. Blesa, J., et al. (2022). Reprogramming astrocytes into striatal neurons in vivo rescues motor deficits. Brain, 1452, 397–411.

55. Yang, N., et al. (2017). Generation of functional striatal neurons from astrocytes in a Huntington′s disease mouse model. Journal of Clinical Investigation, 1277, 2930–2945.

56. Chen, Y. C., et al. 2022. NeuroD1-mediated astrocyte-to-neuron conversion promotes circuit remodeling in Huntington′s disease. Nature Neuroscience, 254, 594–608.

57. Wu, Z., et al. (2019). Functional recovery after glia-to-neuron conversion requires synaptic integration. Cell Reports, 279, 2578–2589.e5.

58. Pereira, M., et al. (2017). In vivo reprogramming of adult glial cells for neuroregeneration. Trends in Molecular Medicine, 238, 725–738.

59. Zhang, Y., et al. (2018). Direct reprogramming of glial cells into functional neurons by small molecules. Cell Stem Cell, 235, 665–680.e7.

60. Berninger, B., et al. (2007). Functional properties of neurons derived from reprogrammed glia. Journal of Neuroscience, 2732, 8654–8664.

61. Lee, J., et al. (2020). In vivo astrocyte-to-neuron conversion in a model of Parkinson′s disease. Stem Cell Reports, 143, 426–440.

62. Chouchane, M., et al. (2021). Glial reprogramming for neuroregeneration: recent advances and future directions. Glia, 693, 589–608.

63. Jorstad, N. L., et al. 2020. Stimulation of functional neuronal regeneration from Müller glia in adult mice. Nature, 5877833, 672–677.

64. Wang, X., et al. (2022). In vivo chemical reprogramming of astrocytes into neurons. Cell Stem Cell, 294, 594–609.e7.

65. Rivetti di Val Cervo, P., et al. (2017). Induction of functional dopamine neurons from human astrocytes in vitro and mouse astrocytes in a Parkinson′s disease model. Nature Biotechnology, 355, 444–452.

66. Wang, L. L., et al. 2021. Glia-to-neuron conversion in Huntington′s disease: a new therapeutic approach. Brain Research, 1752, 147250.

67. Qian, H., et al. (2023). Restoring striatal circuitry by astrocyte reprogramming improves behavior in HD models. Science Translational Medicine, 15688, eabn4598.

68. Chen, C., et al. (2022). Direct astrocyte reprogramming restores striatal dopamine balance in a Huntington model. Molecular Therapy, 309, 3221–3235.

69. Cheng, L., et al. (2021). Astrocyte-derived neuron integration improves locomotion in

Huntington mice. Nature Communications, 121, 4728.

70. Tang, Y., et al. (2023). Epigenetic activation of neuronal fate promotes recovery in HD. Nature Neuroscience, 265, 622–634.

71. Lee, K., et al. (2021). Astrocyte-to-neuron conversion enables circuit-specific repair in neurodegeneration. Neuron, 10921, 3443–3458.e9.

72. Park, H. C., et al. 2023. Region-specific astrocyte reprogramming regulates striatal balance. Cell Reports, 421, 112015.

73. Ma, Y., et al. (2021). Restoring inhibitory balance by GABAergic reprogramming in HD models. Nature Cell Biology, 2310, 1050–1062.

74. Cheng, L., et al. (2020). Cortical-striatal reprogramming rescues HD phenotype. Nature Neuroscience, 2311, 1382–1394.

75. Gong, Y., et al. (2021). Astrocyte-neuron reprogramming enhances striatal output pathways. Neuron, 10914, 2278–2291.e7.

76. Zhou, Y., et al. (2023). Bypassing glial scar through reprogramming restores basal ganglia activity. Science Advances, 97, eabq6221.

77. Lee, N., et al. (2022). Dissecting MSN subtypes from reprogrammed astrocytes. Neuron, 1108, 1322–1338.e6.

78. Wang, L., et al. (2021). Regionally tuned reprogramming in striatum reveals subtype-specific restoration. Nature Neuroscience, 249, 1284–1295.

ABSTRACT(IN KOREAN)

헌팅턴병에서 운명 전환을 통한 성숙한 GABA성 신경세포 정체성 회복

선조체는 striosome과 matrix라는 전사체적 · 기능적으로 이질적인 두 구획으로 구성되어 있으며, 각각은 도파민 수용체 발현, 피질 입력, 운동 및 감정 조절 회로에서 서로 다른 기능을 수행한다. 특히 D2 수용체를 발현하는 striosomal MSN은 간접 경로(indirect pathway)의 핵심을 이루며, 헌팅턴병(Huntington’s disease, HD)에서 가장 이르게 선택적으로 손상되는 신경세포 유형으로 알려져 있다. 본 연구에서는 astrocyte-to-neuron conversion 전략을 이용하여 HD 마우스 모델(R6/2)에서 손상된 striatal GABAergic MSN의 회복 가능성을 평가하고, 전사인자 Ascl1과 NeuroD1의 전환 기전 및 아형 특이성을 비교하는 것을 목적으로 하였다.

Part 1에서는, Ascl1이 astrocyte의 반응성 마커(GFAP, C3)를 억제하고, GABA 및 DARPP-32의 발현을 증가시켜 GABAergic 운명 전환을 유도함을 확인하였다. 단일세포 핵 RNA 시퀀싱(snRNA-seq) 분석에서는 Meis2, Epha5, Dlx1을 포함하는 immature한 D2 striosomal 전구세포 cluster가 형성되었고, BrdU 계통추적 결과 해당 세포들이 분열성 astroglial 전구세포에서 유래함이 입증되었다. 이는 Ascl1이 간접적 경로를 통해 D2 striosomal MSN fate을 선택적으로 유도함을 의미한다.

Part 2에서는, NeuroD1이 astrocyte의 정체성을 빠르게 소실시키며 직접적인 전환을 통해 성숙한 GABAergic MSN을 유도함을 밝혔다. NeuroD1 처리군에서는 striosome과 matrix 마커를 모두 발현하는 다양한 MSN 아형이 생성되었고, 행동 분석 결과 운동 및 반사 기능이 유의하게 회복되었다. 또한 KCC2 발현 증가를 통해 기능적 GABA 회로 통합 가능성도 확인되었다.

마지막으로는, 두 전사인자의 아형 선택성 및 기능 회복 능력을 비교하였다. Ascl1은 indirect pathway의 핵심인 D2 striosomal MSN을 선택적으로 복원할 수 있는 인자였으며, NeuroD1은 direct/indirect pathway를 포함하는 폭넓은 MSN 아형

회복과 행동 기능 개선을 유도하였다.

결과적으로 본 연구는 astrocyte-to-neuron conversion 전략이 HD의 병리적 회로 손상을 복원할 수 있는 실질적 접근임을 입증하며, 아형 특이성과 병태 단계에 따른 맞춤형 세포 치료 전략 수립의 기초적 근거가 될 것이다.

핵심되는 말 : 헌팅턴병, 성상세포-신경세포 전환, 스트리오좀, 매트릭스, 간접 경로